Naval Surface Warfare Center
Carderock Division
West Bethesda, MD 20817-5700

NAVSEA
WARFARE CENTERS
Carderock Division

NSWCCD-50-TR–2010/003 March 2010
Hydromechanics Department Report

A Detailed Study of Transom Breaking Waves: Part II

By
Thomas C. Fu, Anne M. Fullerton, David Drazen, Lisa Minnick, Don Walker,
Toby Ratcliffe, Lauren Russell, and Michael Capitain

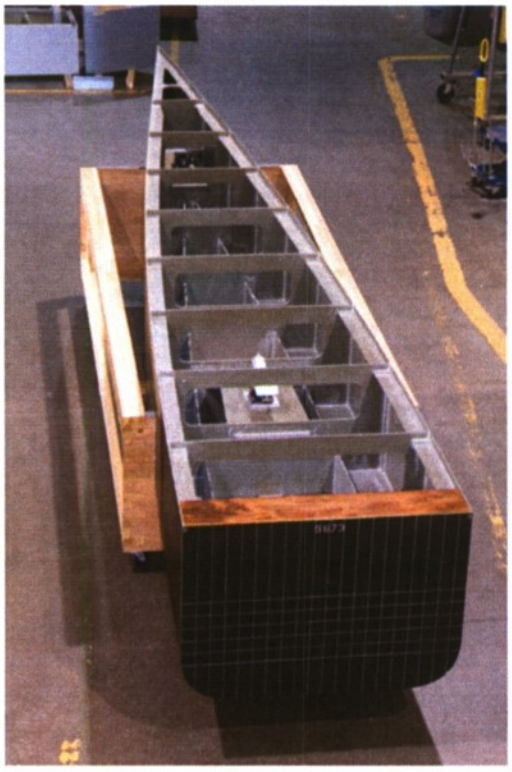

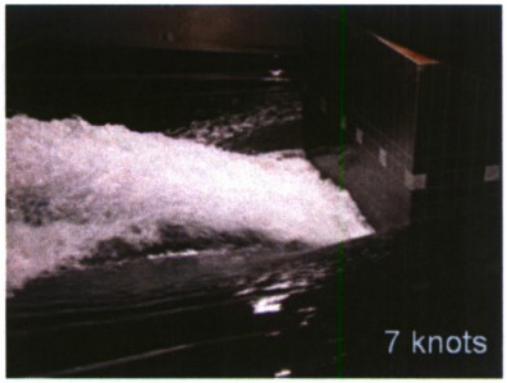

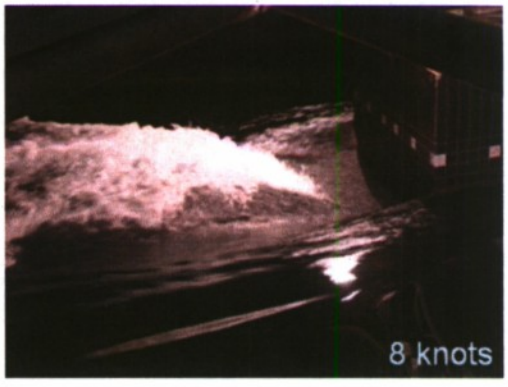

REPORT DOCUMENTATION PAGE

Form Approved OMB No. 0704-0188

1. REPORT DATE *(DD-MM-YYYY)*	2. REPORT TYPE	3. DATES COVERED *(From - To)*
March 2010	Final	March 2010

4. TITLE AND SUBTITLE
A Detailed Study of Transom Breaking Waves: Part II

5a. CONTRACT NUMBER
N0001408WX20046

5b. GRANT NUMBER

5c. PROGRAM ELEMENT NUMBER

6. AUTHOR(S)

Thomas C. Fu, Anne M. Fullerton, David Drazen, Lisa Minnick, Don Walker, Toby Ratcliffe, Lauren Russell, and Michael Capitain

5d. PROJECT NUMBER

5e. TASK NUMBER

5f. WORK UNIT NUMBER
08-1-5600-202

7. PERFORMING ORGANIZATION NAME(S) AND ADDRESS(ES) AND ADDRESS(ES)

Naval Surface Warfare Center
Carderock Division
9500 Macarthur Boulevard
West Bethesda, MD 20817-5700

8. PERFORMING ORGANIZATION REPORT NUMBER

NSWCCD-50-TR-2010/003

9. SPONSORING / MONITORING AGENCY NAME(S) AND ADDRESS(ES)
Dr. L. Patrick Purtell
Office of Naval Research
800 North Quincy Street
Arlington, VA 22217-5660

10. SPONSOR/MONITOR'S ACRONYM(S)

11. SPONSOR/MONITOR'S REPORT NUMBER(S)

12. DISTRIBUTION / AVAILABILITY STATEMENT Approved for public release; distribution unlimited.

13. SUPPLEMENTARY NOTES

14. ABSTRACT

Detailed measurements of the turbulent multiphase flow associated with wave breaking present a unique instrumentation challenge. Measurement systems must be capable of high sampling rates, large dynamic ranges, as well as be capable of making measurements in water, air and optically opaque regions. An experiment was performed on Carriage 2 in the Deep Water Basin at the Naval Surface Warfare Center, Carderock Division, (NSWCCD) in October and November 2008 to measure various characteristics of the breaking wave generated from a ship transom. The primary objective of this work was to obtain full-scale qualitative and quantitative flow field data of a large breaking transom wave over a range of transom drafts and Froude numbers. This test was the second part of a test performed in October 2007.

Several types of measurements were made of the transom stern wave. Sinkage and trim were measured using two string potentiometers. Drag, vertical and side forces were measured using block gages. To quantify the free surface deformation, several techniques were used, including a scanning LiDAR system, laser sheet flow visualization (Quantitative visualization or QViz), Senix Ultrasonic acoustic distance sensors, and high speed video. Additional measurements were made using the Nortek Acoustic Wave and Current (AWAC) profiler, which measured velocity and acoustic

15. SUBJECT TERMS

16. SECURITY CLASSIFICATION OF:			17. LIMITATION OF ABSTRACT	18. NO. OF PAGES	19a. RESPONSIBLE PERSON
a. REPORT	b. ABSTRACT	c. THIS PAGE		52+viii	Anne Fullerton
UNCLASSIFIED	UNCLASSIFIED	UNCLASSIFIED			19b. TELEPHONE NUMBER 301-227-5887

14. ABSTRACT (continued)

backscatter in the water column, and a SonTek Acoustic Doppler Velocimeter (ADV), which measured water velocity. A Defocused Digital Particle Image Velocity (DDPIV) system, which utilizes optical measurements of the flow to measure bubble size, was used to measure the bubble size distribution at a fixed depth aft of the transom. An array of impedance void fraction probes was also used to measure the entrained air at various locations and depths behind the stern.

CONTENTS

FIGURES

TABLES

INTERNATIONAL SYSTEM OF UNITS (SI) CONVERSION LIST

U.S. CUSTOMARY	METRIC EQUIVALENT
1 inch (in)	25.4 millimeter (mm), 0.0254 meter (m)
1 foot (ft)	0.3048 meter (m)
1 pound-mass (lbm)	0.4536 kilograms (kg)
1 pound-force (lbf)	4.448 Newtons (N)
1 foot-pound-force (ft-lbf)	1.3558 Newton-meters (N-m)
1 foot per second (ft/s)	0.3048 meter per second (m/s)
1 knot (kt)	1.6878 feet per second (ft/s) 0.5144 meter per second (m/s)
1 horsepower (hp)	0.7457 kilowatts (kW)
1 long ton (LT)	1.016 tonnes 1.016 metric tons 1016 kilograms (kg) 2240 pounds
1 inch water (60F)	248.8 Pascals (Pa)

ABSTRACT

Detailed measurements of the turbulent multiphase flow associated with wave breaking present a unique instrumentation challenge. Measurement systems must be capable of high sampling rates, large dynamic ranges, as well as be capable of making measurements in water, air and optically opaque regions. An experiment was performed on Carriage 2 in the Deep Water Basin at the Naval Surface Warfare Center, Carderock Division, (NSWCCD) in October and November 2008 to measure various characteristics of the breaking wave generated from a submerged ship transom. The primary objective of this work was to obtain full-scale qualitative and quantitative flow field data of a large breaking transom wave over a range of transom drafts and Froude numbers. This test was the second part of a test performed in October 2007.

Several types of measurements were made of the transom stern wave. Sinkage and trim were measured using two string potentiometers. Drag, vertical and side forces were measured using block gages. To quantify the free surface deformation, several techniques were used, including a scanning LiDAR system, laser sheet flow visualization (Quantitative visualization or QViz), Senix Ultrasonic acoustic distance sensors, and high speed video. Additional measurements were made using the Nortek Acoustic Wave and Current (AWAC) profiler, which measured velocity and acoustic backscatter in the water column, and a SonTek Acoustic Doppler Velocimeter (ADV), which measured water velocity. A Defocused Digital Particle Image Velocity (DDPIV) system, which utilizes optical measurements of the flow to measure bubble size, was used to measure the bubble size distribution at a fixed depth aft of the transom. An array of impedance void fraction probes was also used to measure the entrained air at various locations and depths behind the stern.

ACKNOWLEDGEMENTS

The authors would like to acknowledge the efforts of Susan Brewton, Michael Capitain, James Rice and Connor Bruns (NSWCCD, Code 50), the NSWCCD Media Lab, Eric Terrill and Genevieve Lada (Scripps Institution of Oceanography, UCSD), Kristine Chevalier, Doug Dommermuth, and Donald Wyatt (SAIC), and David Jeon, Daegyoum Kim, and Mory Gharib (California Institute of Technology).

ADMINISTRATIVE INFORMATION

The work described in this report was performed by the Resistance and Propulsion Division (Code 5800) of the Hydromechanics Directorate at the Naval Surface Warfare Center, Carderock Division (NSWCCD). The work was sponsored by the Office of Naval Research under the direction of ONR Program Manager Dr. L. Patrick Purtell (Code 331), performed under contract number N0001408WX20046, and work unit number 08-1-5600-202.

INTRODUCTION

The physics of the transom stern wave continues to be of great importance to understanding both ship breaking waves and bubble wakes. The full-scale breaking transom stern wave is a complex non-linear turbulent flow field, and while Computational Fluid Dynamics (CFD) codes have demonstrated improved capability in predicting the large-scale Kelvin wave structure for a variety of naval craft, the ability of CFD codes to predict the short-scale surface evolution and the energy dissipation involved in breaking regions, spray sheets, and turbulence has not yet been validated and remains a challenge. The primary objective of this work is to obtain full-scale qualitative and quantitative flow field data of a large breaking transom wave over a range of Froude numbers. This experiment was the second part of a test originally performed in October 2007 (Fu, et. al., 1), with the goal of collecting a more detailed data set though under fewer conditions.

The experiment was performed in the Deep Water Basin at the Naval Surface Warfare Center, Carderock Division, (NSWCCD) in October and November 2008 to measure various characteristics of the breaking wave generated from a ship transom. Several types of measurements were made of the transom stern wave. Sinkage and trim were was measured using two string potentiometers. Drag, vertical and side forces were measured using block gages. Several techniques were used to quantify the spray and free surface deformation, including a scanning LiDAR system, laser sheet flow visualization (Quantitative visualization or QViz), Senix Ultrasonic acoustic distance sensors, and high speed video. Additional measurements were made using the Nortek Acoustic Wave and Current (AWAC) profiler, which measured velocity and acoustic backscatter in the water column, and a SonTek Acoustic Doppler Velocimeter (ADV), which measured water velocity. A Defocused Digital Particle Image Velocity (DDPIV) system, which utilizes optical measurements of the flow to measure bubble size, was used to measure the bubble size distribution at a fixed depth aft of the transom. An array of impedance void fraction probes was also used to measure the entrained air at various locations and depths behind the stern.

EXPERIMENTAL APPROACH

Model Description and Facilities

This experiment was performed by towing Model 5673 in the Deep Water Towing Basin on Carriage 2. The basin is approximately 22 feet (6.7 m) deep, 1886 feet (574.9 m) long and 50.96 feet (15.5 m) wide, with a maximum carriage speed of 33.8 ft/s (20 knots) (Saunders, 2). The model was towed using a tow post located 270 in (6.9 m) forward of the aft perpendicular (Figure 1), which was fixed in heave, but free to pitch. A grasshopper linkage was used 90 in (2.3 m) forward of the aft perpendicular to fix the model in yaw, while still allowing the model to pitch about the forward tow post and allowing the stern to heave.

Model 5673 (shown in Figure 2, Figure 3 and Figure 4) has a transom stern and was designed to minimize the generated bow wave so that the transom wake could be more effectively investigated. The model is about 30 feet (9.1 m) long, with a maximum beam of 5 feet (1.5 m). Figure 5 shows a plan view of the model mounted on Carriage 2.

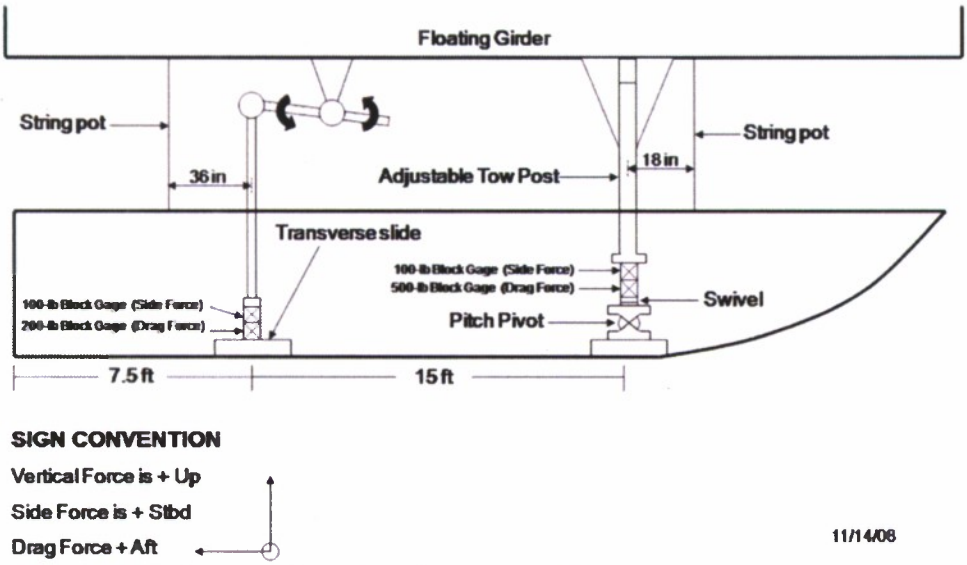

Figure 1. Schematic of transom model tow post and grasshopper setup.

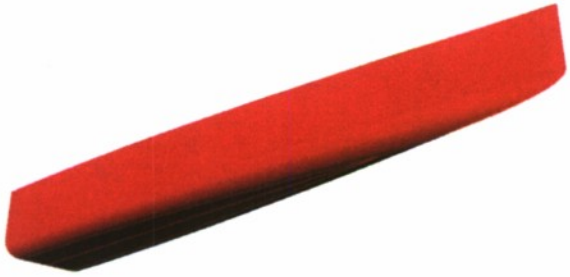

Figure 2. Image of the transom model geometry.

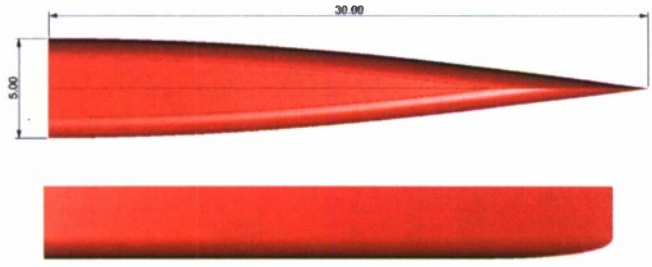

Figure 3. Plan and profile views of the transom model geometry.

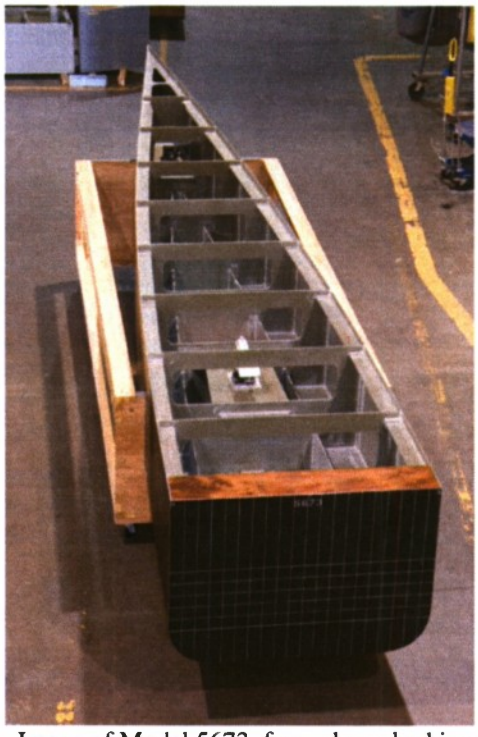

Figure 4. Image of Model 5673, from above looking forward.

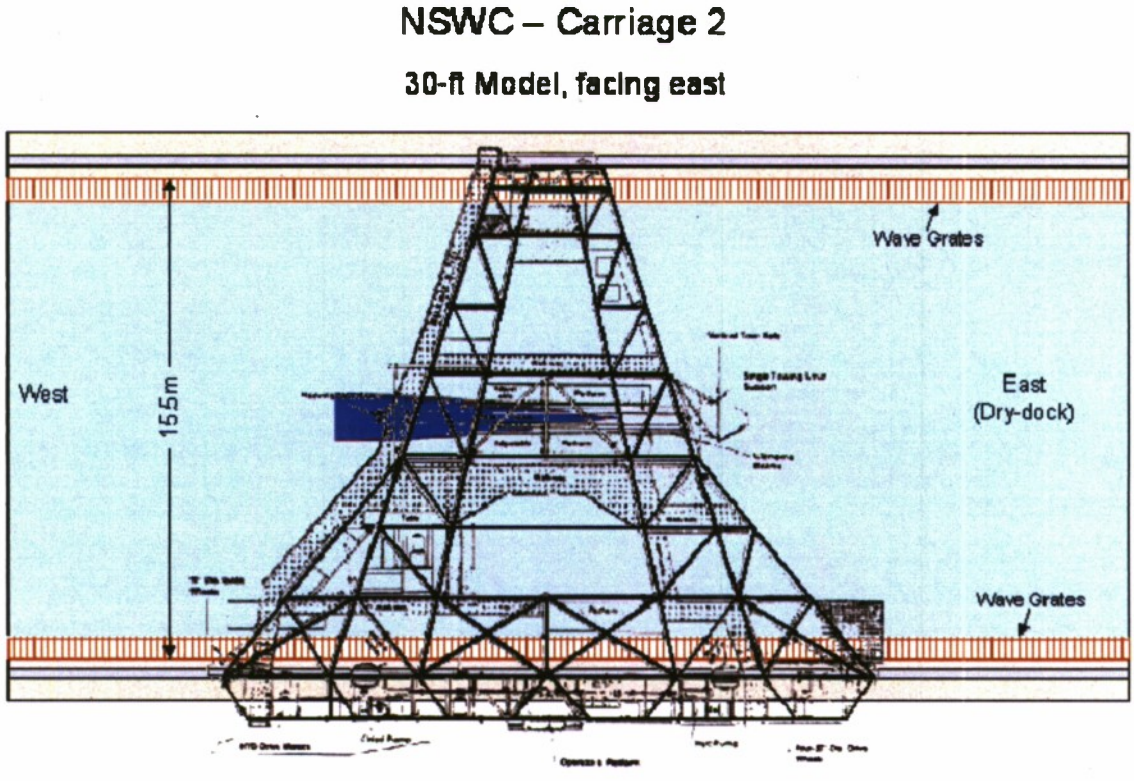

Figure 5. Plan view of model mounted under Carriage 2.

Test Conditions

Model 5673 was tested at 7 knots (wet transom) and 8 knots (dry transom). These conditions were a limited duplicate set from the test conducted the previous year. Table 1 shows the test conditions for both the 2007 and 2008 experiment, along with the length and draft Froude numbers, where length Froude number is defined as:

$$Fn_L = \frac{v}{\sqrt{gL}} \tag{1}$$

and draft Froude number is defined as:

$$Fn_D = \frac{v}{\sqrt{gD}} \tag{2}$$

where v= model velocity

g=gravitational acceleration

L=length of model (30 ft for this model)

D=draft at the transom

Literature suggests that a transom stern vessel will experience a dry stern (also referred to as fully ventilated) at draft Froude numbers above 2.5 (Maki et. al., 3, and Faltinsen, 4). In this experiment, the transom stern is dry at a slightly lower draft Froude number of about 2.11.

Table 1. Test Conditions.

Speed (knots)	Length Froude Number (Fn_L)	Draft Froude Number (Fn_D)	Transom Condition	Test Year
5	0.27	1.4	wet	2007
7	0.38	1.9	wet	2007,2008
8	0.43	2.1	dry	2007,2008
9	0.49	2.3	dry	2007

The model was initially ballasted to the same waterline tested in 2007, with a transom submergence of 1 ft (0.3 m), as shown in Figure 6. Total ballast in the model was 1700 lb (771.1 kg). Dynamic trim was measured using string potentiometers located forward and aft (Figure 1).

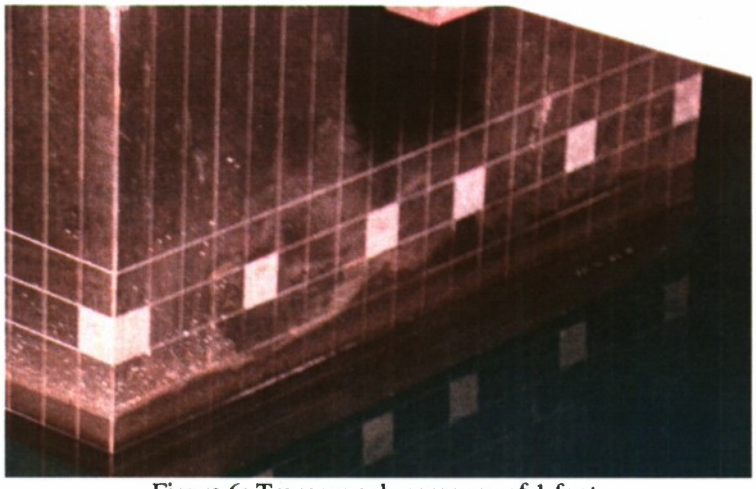

Figure 6: Transom submergence of 1 foot.

Instrumentation

Standard Video and Still Imaging

Three standard frame rate (30 fps) video cameras were used to record the visual appearance of the free surface aft and around the transom model during testing. Two cameras captured the view from the stern looking aft. Another camera was mounted to the carriage to capture the view aft of the model from the port side looking towards the centerline. The last camera was also mounted to the carriage, even further aft of the model on the port side, and was aimed forward toward the centerline and stern. A sketch of these general positions relative to the model is shown in Figure 7.

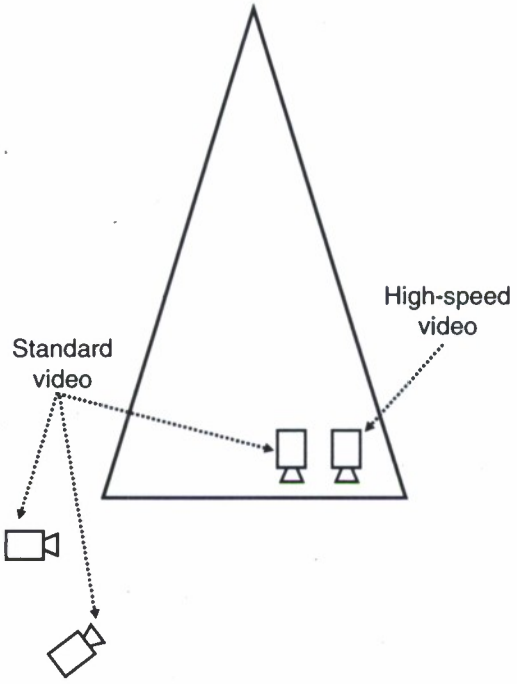

Figure 7. Sketch of standard video camera positions.

High Speed Video

One high speed video camera was used on the starboard side of the model stern. The general camera position is shown in Figure 7. The system is capable of storing 10918 image frames internally before offloading to a computer is necessary. Frame rates of 125, 250, and 500 fps were used yielding recording times of 87 s, 43 s, and 22 s respectively. A fluorescent yellow/green dye (Bright Dyes 106001) was used to visualize the flow around and aft of the transom. A blacklight was used to illuminate the water surface as the dye fluoresces under ultraviolet (UV) light.

Underwater Video

An underwater camera was towed along the port side of the model to capture the underwater flow looking toward the centerline. The camera housing has a built in pan and tilt unit which allowed for adjustment of the camera lens relative to the transom. The camera records at a rate of 30 Hz., and was only deployed during the final phase of the test.

Block Gages

The forward tow set-up included a side force block gage and a drag block gage that were mounted on top of a swivel, allowing the model to yaw slightly in either direction, as shown in Figure 8a. The grasshopper also included a side force block gage and a drag force block gage (Figure 8b).

During the initial testing, a vertical force gage was included in the stack at the forward tow point. After doing a check out run, there was significant twisting in the forward stack from reflected waves in the basin. The reflected waves were larger than

during the 2007 testing since the model was being towed from east to west, which meant that there was no wave dampening from the beach as there was in 2007. The twisting was so severe that it deformed the vertical force gage bracket. The vertical force gage was then removed. The shortened stack appeared to reduce the twisting.

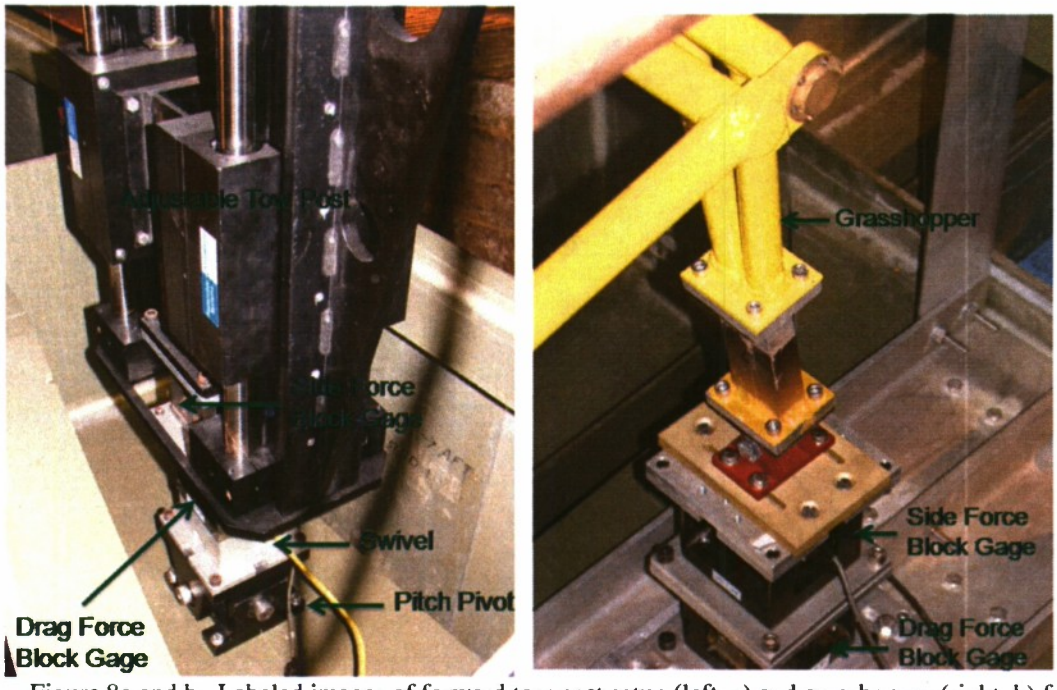

Figure 8a and b. Labeled images of forward tow post setup (left, a) and grasshopper (right, b) for 2008 transom test.

String Potentiometers

Model trim was measured using string potentiometers located at the bow and stern of the model. The distance between the string potentiometers was 234 in (5.94 m). The forward string potentiometer was located 288 in (7.31 m) forward of the aft perpendicular and the aft string potentiometer was located 4.5 ft (1.37 m) forward of the aft perpendicular.

LiDAR

Light Detection And Ranging, or LiDAR, is a remote sensing system used to collect topographic data. The LiDAR system (Riegl LMS-Q140-80i) used contains a single pulsed infrared (900 nm) laser scanner and a three-sided mirror which rotated to deflect the laser at different angles along a single line. The time for the reflected pulse to echo back to the sensor receiver is used to calculate distance. The range accuracy of the LMS-Q140-80i unit is +/- 1 in (2.54 cm) for highly reflective surfaces. The instrument scans an angular region of +/- 40 degree at a maximum line sample rate of 40 Hz. The laser pulse frequency is 30 kHz and the measurements are spread at equal angles along the scan line. As infrared radiation is absorbed by water, we only expect a small fraction of the incident energy to be scattered back to the instrument. At large off-nadir angles, no

signal will be returned and the actual extent of the scan region will be less than its theoretical maximum.

The primary goal of the LiDAR system's measurement was to capture the statistical properties (mean and standard deviation) of the transom wake. A set of secondary goals to further characterize the structure of the wake was developed if sufficient time allowed. The LiDAR system was mounted to a traverse which moved in a longitudinal direction parallel to the centerline of the model. It was mounted on a pan and tilt unit which allowed for remote control of the position of LiDAR during testing. The system was tested in four different configurations, referred to as Fixed (A), Moving (B), Parallel (C), and Panning (D). The first configuration was similar to that tested in 2007, where the LiDAR system was set in a fixed position for each run and scanned in a line parallel to the stern. Data was collected at 40 Hz for both speeds with the system in three different positions under this configuration, which included 40.125 in (1.02 m), 52.125 in (3.2 m), and 64.125 in (1.63 m) aft of the transom, shown in Figure 9 as A-Fixed. The LiDAR centerline was 5.625 in (0.14 m) port of centerline of the model, and the mean height of the LiDAR system was 15.78 ft (4.8 m) off the still waterline.

In the second configuration (B-Moving), the LiDAR system also scanned in a line parallel to the stern. Instead of measuring at a fixed location, the LiDAR system moved along the traverse at a constant speed of 1.46 in/s (3.71 cm/s). The extent of the region was from 16.125 in (0.41 m) aft of the stern to 86.125 in (2.19 m) aft of the stern during one run, allowing for scans at a greater number of longitudinal locations, as shown in Figure 9. Data was collected at a rate of 20 Hz at both speeds for three runs in this configuration. The LiDAR centerline was again 5.625 in (0.14 m) port of centerline of the model, and the mean height of the LiDAR system was 15.78 ft (4.8 m) off the still waterline.

In the third configuration, Parallel-C, the LiDAR system was rotated to be parallel to the model and was scanning along a line that moved from 124 in (3.15 m) forward of the stern to 194 in (4.93 m) aft of the stern. The scan line was located 9.644 in (0.24 m) port of centerline of the model, as shown in Figure 9. Data was collected at both 20 and 40 Hz.

In the panning configuration, Panning-D, the LiDAR system was mounted parallel to the stern. In this configuration it was mounted at the highest location on Carriage 2, about 28.5 ft (8.7 m) off the still waterline. The system was then tilted from looking straight down at the water surface to an angle of 90^{o} relative to the water surface at a rate of 3 degrees per second. This resulted in a full surface map of the wake behind the stern. The LiDAR sweep covered the area from the vertical rails all the way to the eastern wall of Carriage 2 centered at about 5.5 in (0.14 m) port of the centerline of the model. Since the area of concern is the region close to the model, the distance aft of the transom was limited to about 60 ft (18.3 m) .

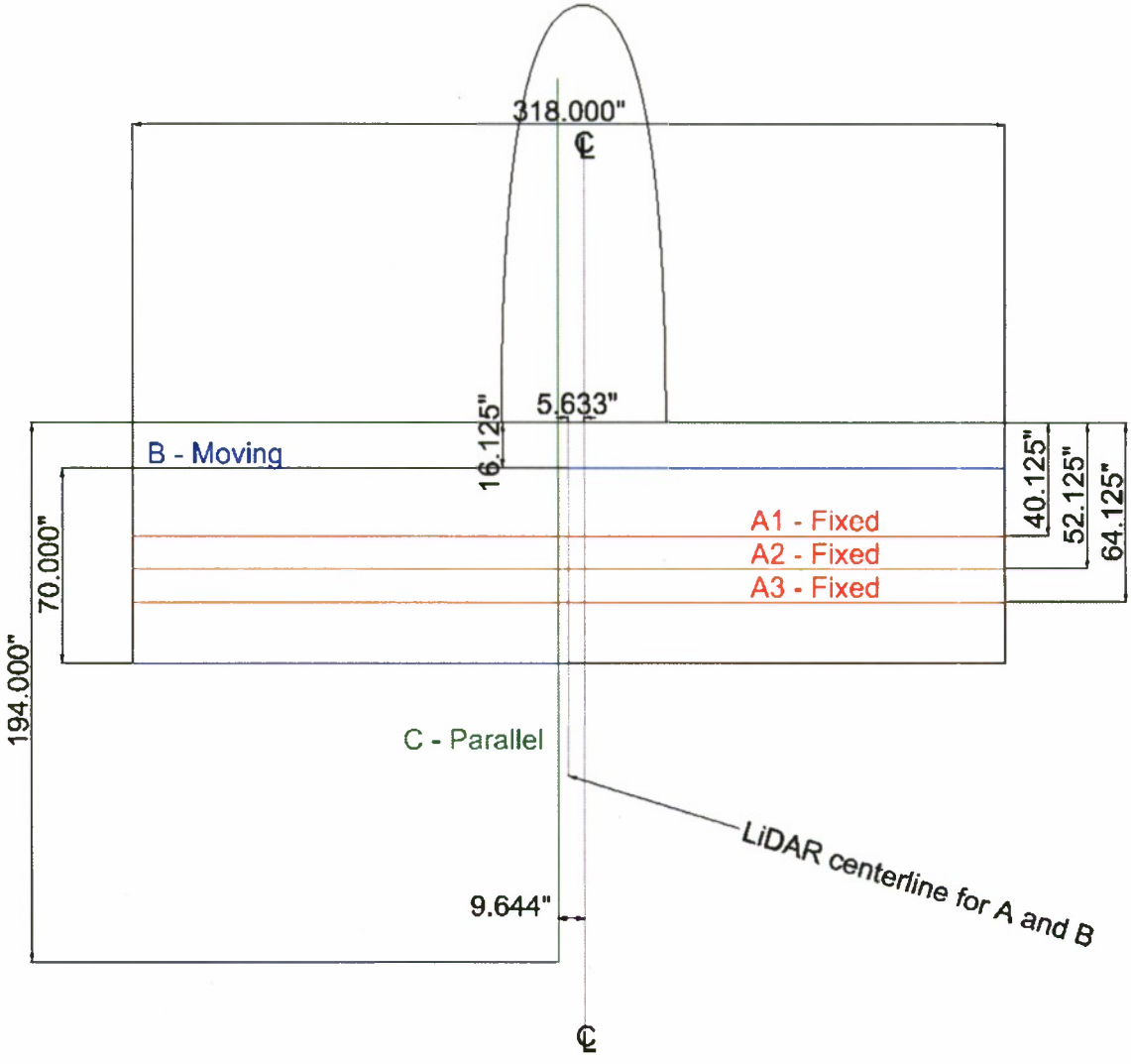

Figure 9. Plan view sketch of LiDAR measurement configurations. The along-scan lengths for A – Fixed, B – Moving, and C – Parallel are theoretical based on the scan extent and the height of the LiDAR off the free surface. The actual length will depend on the nature of the reflective surface.

QViz

The Qviz system, shown in Figure 10, consists of a 3 watt laser (532 nm wavelength) fed through a fiber-optic cable routed to an enclosed housing containing a cylindrical lens, mounted at the desired projection location (A in Figure 10). The cylindrical lens converts the laser beam into a light sheet, which is projected perpendicular to the disturbed free surface. Video cameras (B, C) collect digital images of the resulting intersection, representing instantaneous cross-sections of the wave shape. The physical position of the cameras with respect to the laser projection housing is held fixed, and the entire assembly is moved longitudinally behind the model transom using a

motorized traverse. The detailed system operation was similar to previous versions of the QViz system, details of which are given in Furey and Fu (5) and Rice et al. (6).

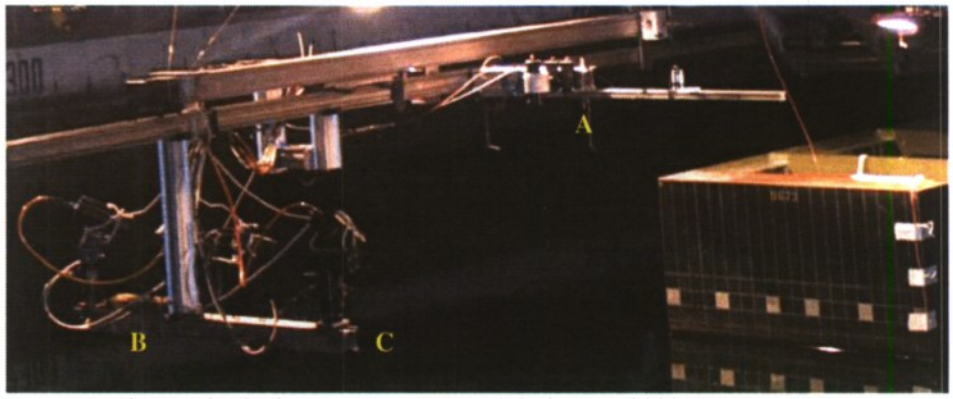

Figure 10. QViz system as mounted during the 2008 Transom Test.

The QViz system acquired cross-sections spanning roughly 10 to 30 inches (0.25 – 0.76 m) port of the model centerline, with resolution on the order of one hundredth of an inch (0.025 cm). The transverse cuts were nominally obtained at 1 inch (0.025 m) increments, resulting in a measurement area spanning 1 inch to 48 inches (0.025 to 1.22 m) aft of the transom.

Senix Ultrasonic Sensors

One Senix ToughSonic Ultrasonic sensor, which is a non-contact, acoustic instrument for measuring distances through air, was used to collect longitudinal water level data aft of the model. The sensor was mounted to the QViz traverse and data was collected at static locations aft of the stern for about 10 seconds and along the traverse at a steady speed. The sensor was located 0.3125 in (0.8 cm) starboard of centerline of the model, and was traversed from the stern to 44.625 in (1.13 m) aft of the stern.

Four Senix ToughSonic Ultrasonic sensors were used to collect longitudinal wavecut data. A truss section (wave boom) cantilevered from the basin wall over the water, provided a structure on which the sensors were mounted, shown in Figure 11. The wave boom extends 22.4 ft (6.83 m) from the basin wall, which places the end of the wave boom approximately 3 ft (0.91 m) short of the basin centerline. The four sensors were mounted on a stock of 80-20 extrusion (to be referred to as the "sensor beam") clamped to the wave boom. In this way, the sensor positions could be changed by simply sliding the sensor beam along the wave boom. A photosensor was set to trigger data collection when the forward perpendicular of the model was 24.979 ft (7.61 m) from the sensors.

Wave elevation data was collected at a sample rate of 20 Hz. The transverse locations for the sensors, measured outboard from the model centerline are listed in Table 2 in inches and in non-dimensional y/B locations (distance outboard divided by the transom beam).

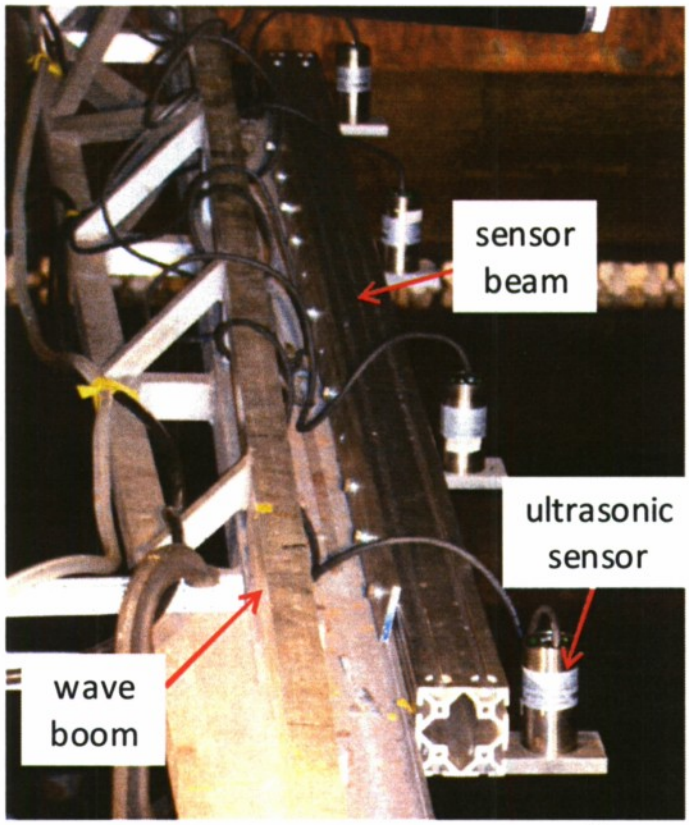

Figure 11. Ultrasonic sensors and sensor beam mounted to wave boom. The view is outboard from the model centerline.

Table 2. Five (5) ultrasonic sensor position configurations.

	1		2		3		4		5	
	inches	y/B	inches	y/B	inches	y/B	inches	y/B	inches	y/B
Sonic 1	51.75	0.86	57.75	0.96	63.75	1.06	69.75	1.16	75.75	1.26
Sonic 2	82.25	1.37	88.25	1.47	94.25	1.57	100.25	1.67	106.25	1.77
Sonic 3	112.5	1.88	118.5	1.98	124.5	2.08	130.5	2.18	136.5	2.28
Sonic 4	142.25	2.37	148.25	2.47	154.25	2.57	160.25	2.67	166.25	2.77
Notes	initial configuration		+ 6"		+ 12"		+ 18"		+ 24"	

Acoustic Wave and Current Profiler (AWAC)

The Nortek Acoustic Wave and Current Profiler AWAC is an acoustic Doppler current profiler with some added features. In addition to the three acoustic beams angled at 25 degrees from vertical as typically found on an ADCP, the AWAC system has a dedicated vertical center beam which is used to measure the water surface through Acoustic Surface Tracking (AST). This center beam transmits a short acoustic pulse that can be finely resolved, allowing for free surface waves of short periods to be accurately measured. The acoustic return at a fine vertical resolution may be correlated to the entrained air in the water. The AWAC is capable of sampling at 4 Hz to capture the surface level; if all bins are recorded to acquire acoustic return through the water column,

the sampling frequency is limited to 2 Hz. The AWAC (Figure 12) was stationary during the testing, on a bottom mount about halfway along the length of the tank, located near the wave boom location which held the ultrasonic sensors. Measurements were made for both speeds tested while the AWAC was bottom mounted under the centerline of the model, as well as 2.5 ft (0.76 m) and 5 ft (1.52 m) (half-beam and full beam) starboard of centerline. These locations were chosen to both overlap and augment the measurements taken during the 2007 testing.

Figure 12. Nortek Acoustic Wave and Current Profiler (AWAC) on bottom mount.

Defocused Digital Particle Image Velocimetry (DDPIV)

A research group from California Institute of Technology used a Defocused Digital Particle Image Velocimetry System (DDPIV) to quantify the bubbles generated in the wake of the transom model. DDPIV can be used to optically measure bubble size statistics in a large volume, and can be made rugged enough to be placed in a turbulent flow environment. The test rig used in the 2007 test was modified to be mounted on the carriage via the Cieslowski bracket. The system measured bubbles for the entire run instead of being fixed in position and making measurements as the model passed, as it was during the 2007 testing. The DDPIV housing was attached to the vertical rails on the east end of the carriage. In addition, the laser delivery system (separate from the laser for QViz) was modified for the new arrangement. A new fiber optic system was developed to bring the laser beam underwater and into the probe volume for 2008 test, as opposed to the previous system, which employed a large cylindrical vessel underwater to house a steering mirror and lens, which was too large to be towed effectively. Figure 13 shows the DDPIV system configuration.

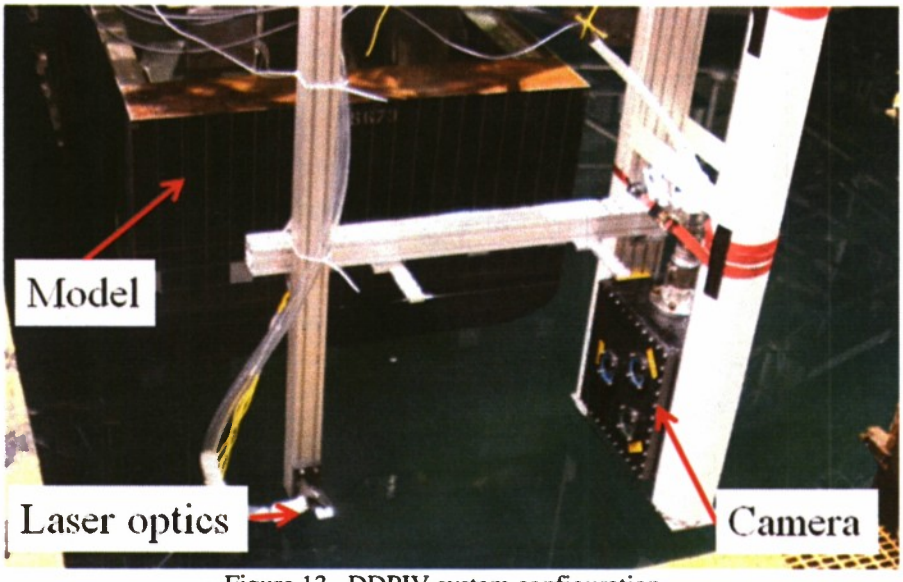

Figure 13. DDPIV system configuration.

Void Fraction Probes

A set of six impedance void fraction probes were used to measure the fraction of air in the transom stern wake. The goal of the 2008 testing was to improve the design of the void fraction probe electronics and evaluate the results against the 2007 void fraction data. The physical design of the probe did not change between 2007 and 2008, but the electronics associated with the probes was improved to reduce noise in the measurement. and is based on a design developed by Waniewski (7).

The probes consist of two concentric stainless steel electrodes separated by insulation as shown in Figure 14. The outer electrode is a 13 gauge stainless steel tube with an outer diameter of 0.095 in (0.24 cm) and a thickness of 0.005 in (0.013 cm). The inner electrode is a stainless steel spring wire with a 0.24 in (0.61 cm) diameter. The inner electrode was insulated from the outer electrode using heat shrink tubing and then fitted inside the stainless steel tube. The stainless steel tube was then placed inside a 0.125 in (0.32 cm) diameter brass tube that was 6 in (15.24 cm) in length. Glue lined heat shrink tubing was used to secure the connection between the brass tubing and stainless steel tube.

The outer electrode is grounded and a sinusoidal voltage signal of ±2.5V with an excitation of 500 kHz applied to the inner electrode. The impedance across the two electrodes increases with increased void fraction (% of air) and is mainly resistive for excitation frequencies below the megahertz level. When a bubble is pierced by a probe the current between the two electrodes decreases and voltage output of the probe is a large negative spike. The sampling rate of the probes was set at 20 kHz and was determined based on limitations of the data acquisition system.

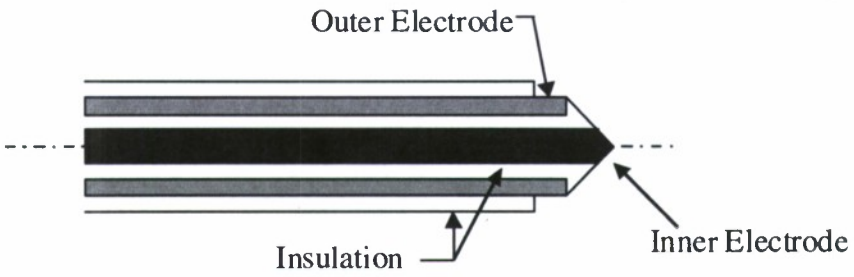

Figure 14. Cross section schematic of void fraction probe.

The probes were mounted in a brass strut with a vertical separation of 3.5 in (9 cm) between probes, see Figure 15. Aluminum plates were used to attach the strut to a traverse that allowed for the longitudinal position of the probes relative to the transom to be controlled. The traverse was aligned with the model centerline and allowed for a longitudinal testing range of about 8 ft (2.4 m). The traverse was attached to the vertical rails on the carriage using the Cieslowski bracket, which allowed for adjustment of the vertical position of the probes. Data was collected with the probe array at three vertical positions, providing a vertical resolution of 1.75 in (4.5cm). Table 3 provides a summary of probe heights relative to calm water for each vertical position.

Figure 15. Void fraction probes on brass strut.

Table 3. Probe heights relative to calm water. Negative numbers refer to locations below the calm water line, positive numbers above.

	Height (in)		
Probe #	Vertical Position 1	Vertical Position 2	Vertical Position 3
6	7.5	11	9.25
5	4.0	7.5	5.75
4	0.5	4.0	2.25
3	-3.0	0.5	-1.25
2	-6.5	-3.0	-4.75
1	-10	-6.5	-8.25

Table 4 shows the void fraction test matrix. Due to time constraints, data was only collected at the 8 knot dry transom condition. Having all six probes operating at once on the carriage created a larger amount of electronic noise than was observed in the calibration lab prior to the test. To minimize this noise, only two or three probes were operated concurrently. These probe combinations are noted in the test matrix. Data was collected at seven longitudinal locations. Three longitudinal locations aft of the stern (x=41 in (1.0 m), x=46 in (1.2 m), and x=56 in (1.4 m)) are locations for which 2007 data exists. The data collected in 2008 focused on two areas of the rooster tail: its crest and close to its inception where the 2007 data suggested that a smaller measurement spacing would be beneficial in understanding the flow.

Table 4. Void fraction test matrix.

Speed	Longitudinal Location	Vertical Position	Probes
(kts)	(in aft of stern)		
8	41.0	1	2,3
8	43.5	1	2,3
8	41.0	3	1,2
8	43.5	3	1,2
8	46.0	3	1,2
8	50.5	1	3,4
8	53.5	2	3,4,5
8	56.0	2	3,4,5

RESULTS

Figure 16 shows still images recorded of the transom wake during testing over at 7 and 8 knots. At 7 knots the transom is wet and the region close to the transom is dominated by a large amount of entrained air. Initial analysis of additional footage suggests that there is a recirculation region set up on either side of the model centerline. Inspection of the right hand side of Figure 17 shows that the dye injected at ¼ beam from the centerline flows outward along the transom before heading aft the transom edge. This behavior is also confirmed from visual inspection of the video data and actual wake. At a speed of 8 knots the entire transom is dry and the rooster tail begins to form 2 to 3 ft aft of the transom. The wake is well defined, narrow, and quickly steepens to a defined peak where it begins to spill out and widen.

Figure 17 and Figure 18 show still images from the standard video of the dye injection at the starboard corner of the stern and at ¼ beam starboard of centerline for 7 knots and 8 knots, respectively. The dye path gives some insight to the flow path at the two conditions, further analysis is ongoing.

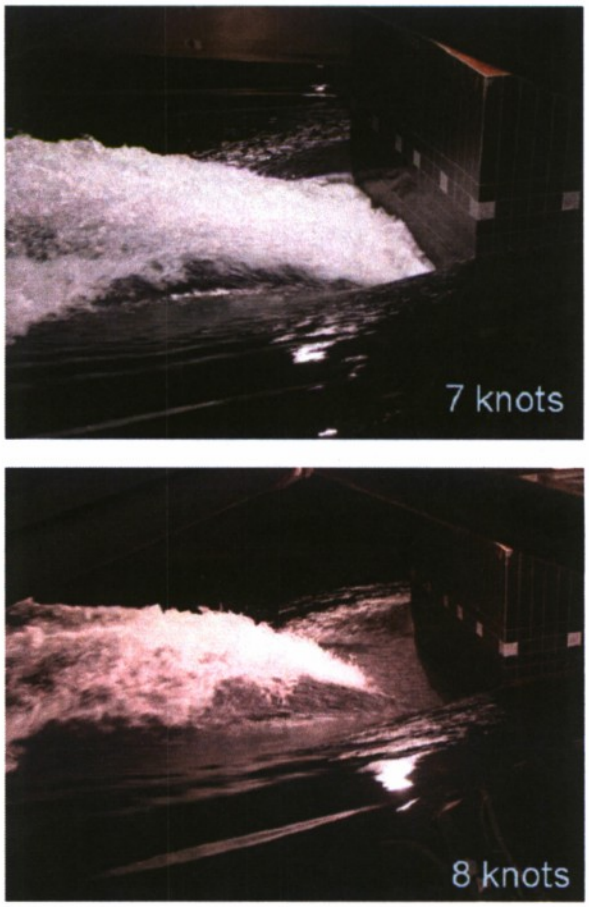

Figure 16. Still images of transom wake during testing for all tested speeds.

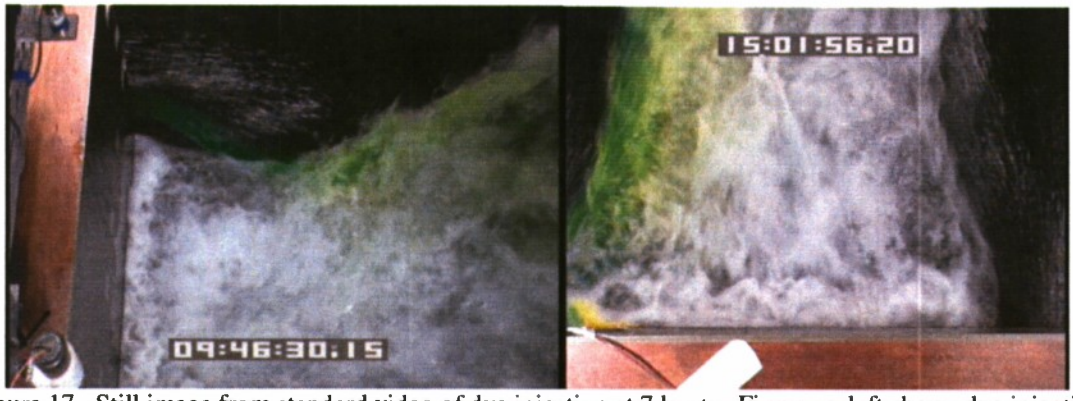

Figure 17. Still image from standard video of dye injection at 7 knots. Figure on left shows dye injection at starboard edge of transom, right shows dye injection at ¼ beam starboard of centerline.

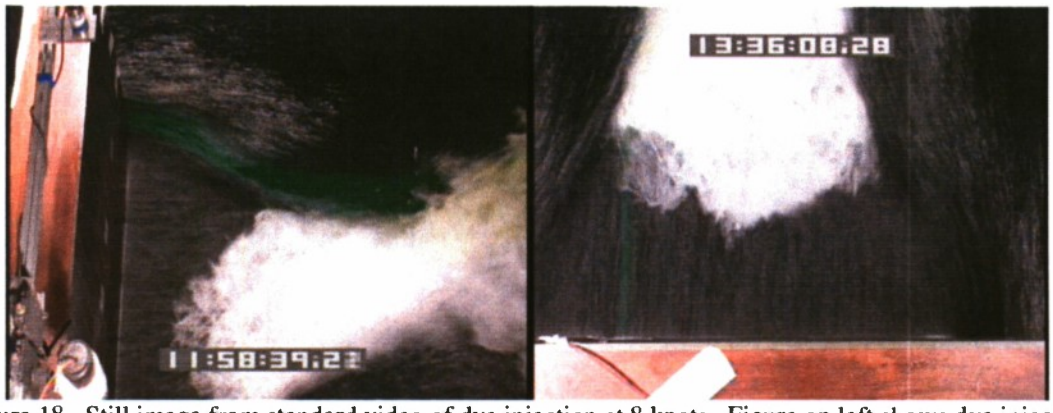

Figure 18. Still image from standard video of dye injection at 8 knots. Figure on left shows dye injection at starboard edge of transom, right shows dye injection at ¼ beam starboard of centerline.

High Speed Video

Figure 19 shows still images recorded by the high speed video of the dye injection at the starboard corner of the stern for 7 knots (left) and 8 knots (right). Again, the dye path gives some insight to the flow path at the two conditions.

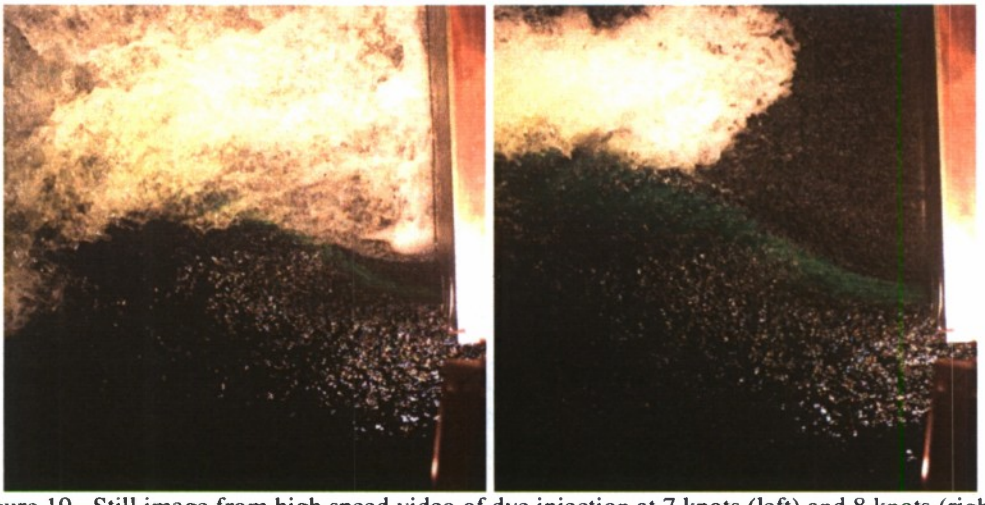

Figure 19. Still image from high speed video of dye injection at 7 knots (left) and 8 knots (right).

Underwater Video

Near the end of the test period, some underwater video was collected in an effort to see how it could help in the understanding of the structure of the wake, see Figure 20. The camera was placed on the port side of the model and the field of view (FOV) adjusted to include the entire transom. No video was captured for the 8 knot case. The transition on the left hand side of the figure from clear to cloudy water denotes the location of the waterline on port side of the transom. Figure 21 is a calibration image showing the location of the dye injection and should help in interpreting Figure 20.

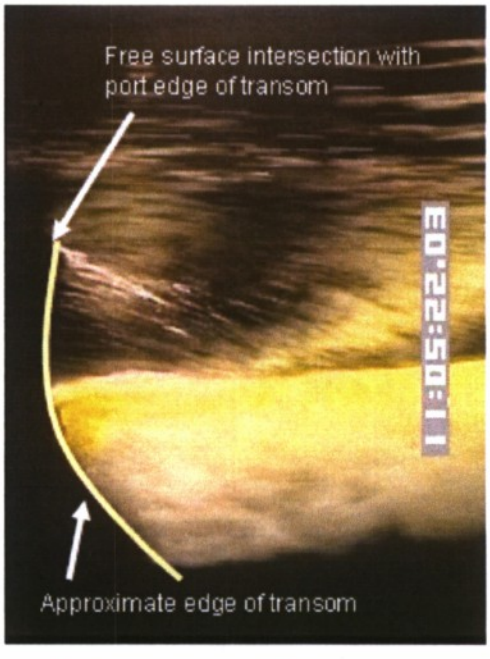

Figure 20: A still from the underwater camera at a model speed of 7 knots View is from slightly below transom looking towards starboard. Flow is from left to right. The transition from clear to cloudy (i.e. high void fraction) shows where the water line at the transom is. Dye injected at one quarter beam in from the port edge of the transom can be seen to flow out to the edge of the transom.

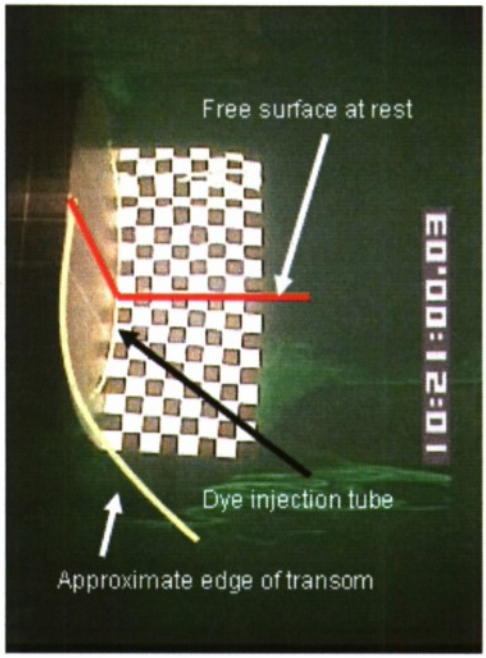

Figure 21: A still image from the underwater camera video showing the location of the transom within the camera's field of view. The location of the dye injection, the still free surface and the edge of the transom are denoted in the image.

Forces

Drag forces, side forces, and heave displacement at the bow and stern were averaged over all runs for each speed. The results are included in Table 5. For the 2008 data, the distance between the string potentiometers was 234 in (5.94 m). The forward string pot was located 288 in (7.31 m) forward of the aft perpendicular and the aft string pot was located 48.5 in (1.37 m) forward of the aft perpendicular. Table 6 shows the same force and displacement results from the 2007 test for comparison. Note that aft drag (on the grasshopper) was not measured during the 2007 testing. For the 2007 testing, the distance between the string potentiometers was 216.8125 in (5.5 m). The forward string pot was located 288.125 in (7.3 m) forward of the aft perpendicular and the aft string pot was located 71.3125 in (1.8 m) forward of the aft perpendicular. In all cases drag increases with increased speed, as expected. Side forces stayed within the allowable range of 1-2% of drag force.

Figure 22 shows a comparison of the drag results from 2007 and 2008. There were slight differences in the average drag results with a 5.8% difference at 7 knots and a 5.4% difference at 8 knots. Table 7 shows the calculated trim angle and draft at the forward and aft perpendiculars for the 2007 and 2008 data. The trim angle appears to be increasing with increased speed. Differences in trim angle from 2007 to 2008 are small, within about a tenth of a degree. Differences in draft are also small, on the order of hundredths of feet (tenths of inches).

Table 5. Summary of average and standard deviation of forces and heave at each speed for 2008 test.

		Fwd Drag (lb)	Aft Drag (lb)	Fwd Side Force (lb)	Aft Side Force (lb)	Bow Heave (in)	Stern Heave (in)
7 kts	Average	230.24	-0.22	-1.38	2.91	-0.15	1.81
	Std Dev	2.54	0.03	0.63	0.40	0.02	0.06
8 kts	Average	282.47	-0.32	-2.12	3.32	-0.22	2.53
	Std Dev	1.48	0.03	0.95	0.33	0.03	0.05

Table 6. Summary of average and standard deviation of forces and heave at each speed for 2007 test.

		Fwd Drag (lb)	Fwd Side Force (lb)	Aft Side Force (lb)	Bow Heave (in)	Stern Heave (in)
5 kts	Average	95.84	0.74	-2.38	-0.07	0.66
	Std Dev	0.67	0.26	0.32	0.01	0.06
7 kts	Average	216.77	1.71	-4.08	-0.16	1.77
	Std Dev	1.43	0.39	0.96	0.04	0.06
8 kts	Average	267.22	2.24	-5.43	-0.25	2.49
	Std Dev	0.61	0.44	0.43	0.03	0.07
9 kts	Average	295.66	2.09	-6.21	-0.31	2.64
	Std Dev	2.31	0.77	0.72	0.02	0.11

Table 7. Calculated trim angle and draft for 2007 and 2008 data.

Speed	Fn_L	Trim Angle	T_{FP}	T_{AP}	Fn_D	Trim Angle	T_{FP}	T_{AP}	Fn_D
		2008				*2007*			
(kts)		(deg)	(ft)	(ft)		(deg)	(ft)	(ft)	
5	0.27	n/a	n/a	n/a	n/a	0.19	0.97	1.08	1.43
7	0.38	0.48	0.94	1.19	1.91	0.51	0.93	1.20	1.90
8	0.43	0.67	0.91	1.26	2.12	0.73	0.90	1.29	2.10
9	0.49	n/a	n/a	n/a	n/a	0.78	0.90	1.31	2.34

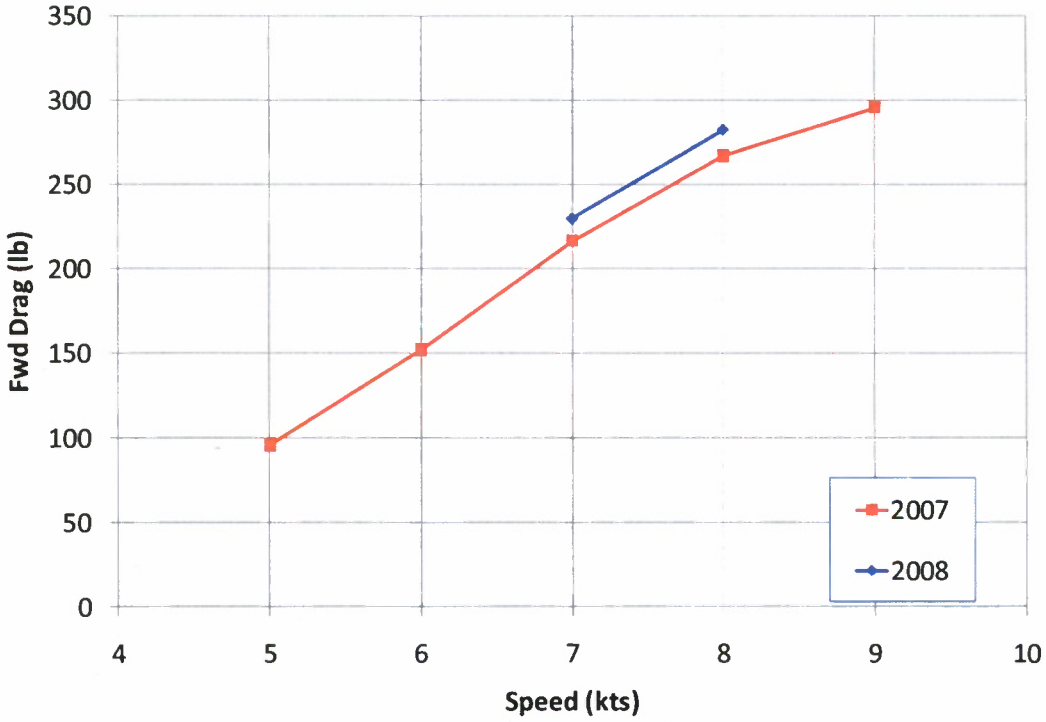

Figure 22: Drag comparison between 2007 and 2008.

LiDAR

The LiDAR system measures along a line with data points having an equal angular spacing, which causes the points near the center to be more closely spaced than those at the edge. Prior to analysis the data was binned so it would have equal spacing between measurements. For the measurements where the LiDAR was held fixed at a location aft of the transom (see configuration A in Figure 9), a spacing of 2 inches was used. The data within each bin was averaged and any bin with no data was set to be "not a number" (NaN). The temporal mean and standard deviation of the binned data is shown in Figure 23 and Figure 24. The total experimental time over which those means and standard deviations were computed are given in Table 8.

Data returned from the case where the LiDAR was moving at a constant rate along the traverse (see configuration B in Figure 9) is shown in Figure 25 for a speed of 7 knots and Figure 26 for a speed of 8 knots. The data was binned in the direction parallel to the transom with a spacing of 1.5 inches. The speed of the traverse and the scan rate of the LiDAR yields a spacing of 0.07 inches between successive scan lines. Data is not binned in the direction aft of the transom. In Figure 25, the mean and the standard deviation of three runs are presented on the left and right hand sides, respectively. For Figure 26, the mean and the standard deviation of five runs are shown. The standard deviation of the wake elevation for both speeds appears to be similar outside of the edges of the wake where there are steep gradients. As the uncertainty in the LiDAR range is ±1 inch, the standard deviations presented are not unreasonable.

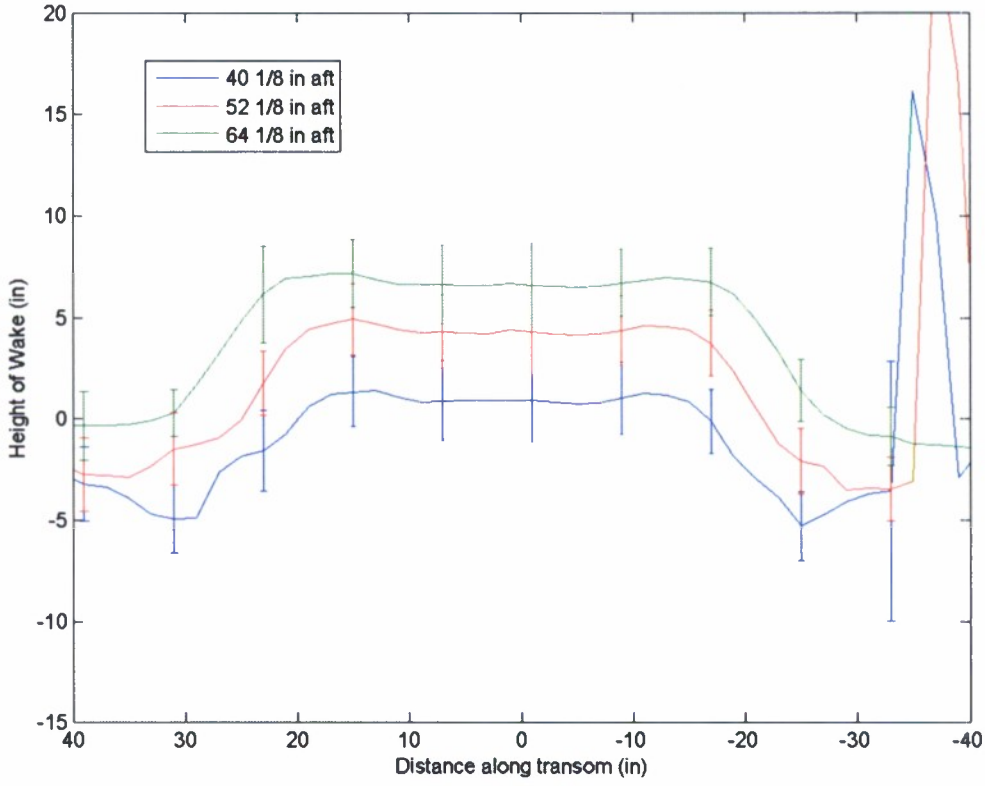

Figure 23: Mean height of wake at 7 knots as measured by the LiDAR at three diserete locations aft of the transom. The error bars denote the standard deviation of the measurement during the three runs. The distanee along the transom is positive to starboard. The signal seen at -35 inches is due to the LiDAR measuring the distanee to the QViz traverse. The data has been binned into horizontal segments with a width of 2 ineh es.

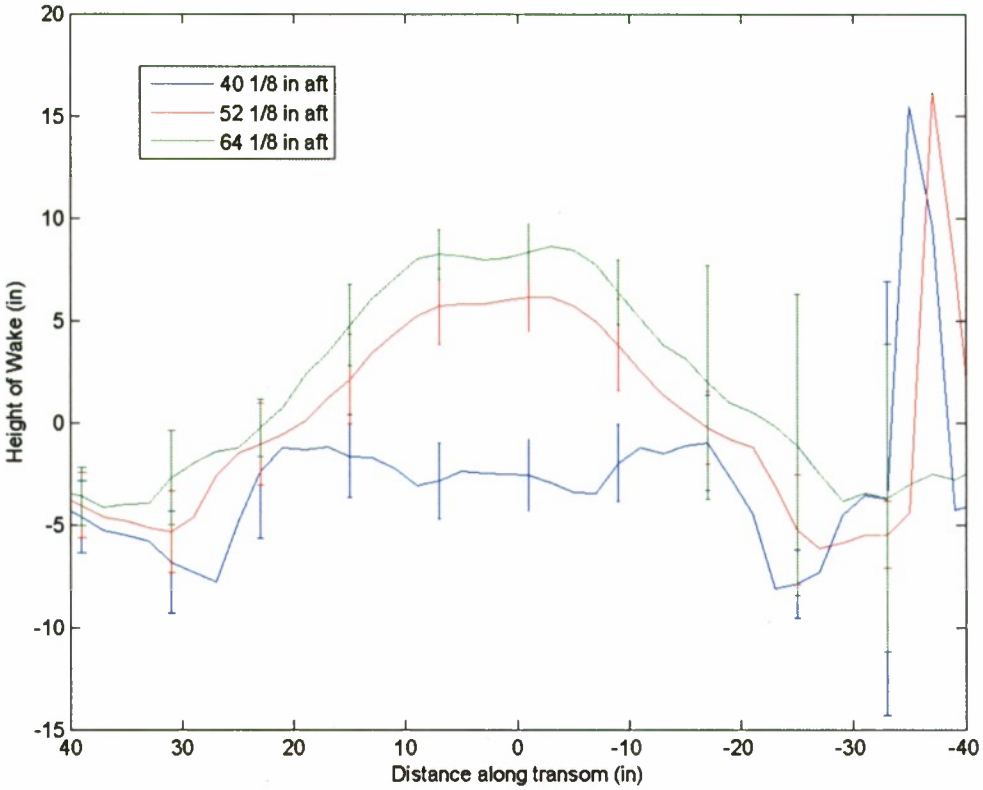

Figure 24. Mean height of wake at 8 knots as measured by the LiDAR at three discrete locations aft of the transom. The error bars denote the standard deviation of the measurement during the three runs. The distance along the transom is positive to starboard. The signal scen at -35 inches is duc to the LiDAR measuring the distance to the QViz traverse. The data has been binned into horizontal segments with a width of 2 inches.

Table 8. Total amount of data used to generate the mean and standard deviations shown in Figure 23 and Figure 24. These represent concatenations of approximately 3-6 separate runs.

	Distance aft of transom		
Speed (knots)	40.125 in	52.125 in	64.125 in
7	202s	321s	318s
8	137s	192s	119s

The primary objective of the LiDAR measurements was to better understand the mean and standard deviation of the wake height, which was accomplished by LiDAR configurations A and B. After all of the data for the primary objectives was collected, measurements for secondary objectives were conducted for LiDAR orientations C and D. Only one run for each speed was collected in each of these configurations. Figure 27 and Figure 28 show the time averaged wake height for the parallel LiDAR orientation, C. The total fraction of dropouts in the time series measured at a fixed distance aft of the transom is also shown. We see that past 100 in (2.54 m) there is a drop in the wake height, which

is attributed to an undersampling of the wake, due to the large number of dropouts. These dropouts may be caused by a large angle of intersection between the incident laser pulse and the free surface, which allows only a small fraction of the incident energy to return back to the instrument. There could also be insufficient surface roughness to scatter enough energy back to the instrument. Close to the transom the LiDAR does not perform well and causes spikes in the data. Some of these spikes may be reduced with further data, but the dropouts are likely due to the nature of the scattering surface. At 7 knots, this region is mainly foam and the behavior of the LiDAR when scattering off of this surface is not well understood. At 8 knots, the region is devoid of foam and is therefore dependent on surface roughness to scatter the laser energy back.

Figure 29 and Figure 30 are images representing the amplitude of the measured LiDAR signal when in the panning configuration D. The value is non-dimensional and is simply an 8-bit number representing the relative strength of the returned signal to the emitted pulse. While the amplitude does not directly represent the wake height, we can clearly see the spatial structure of the wake as the signal is scattered by foam, bubbles and surface roughness induced by the wake itself. Further work on obtaining the wake height from the measured data is ongoing.

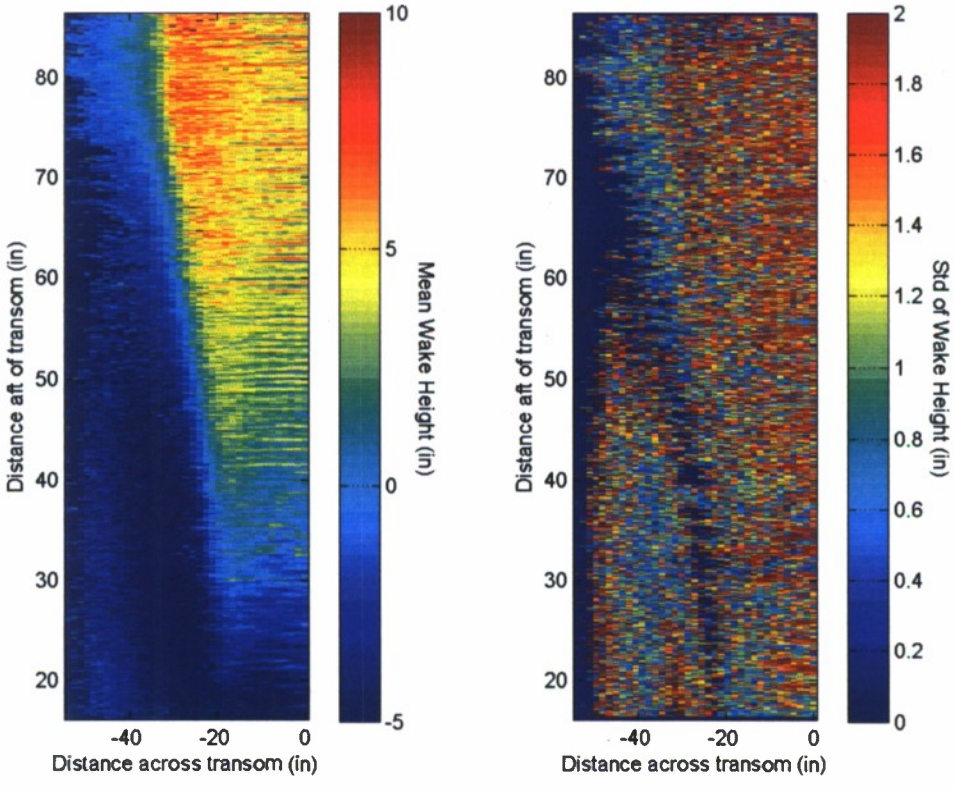

Figure 25. Surface plots of the mean and standard deviation of the wake height at a speed of 7 knots. The figure on the left is the mean wake height after it has been binned along a scan into bins of width 1.5 inches. The figure on the right is the standard deviation of the height. The statistics were computed over three repeats of each speed.

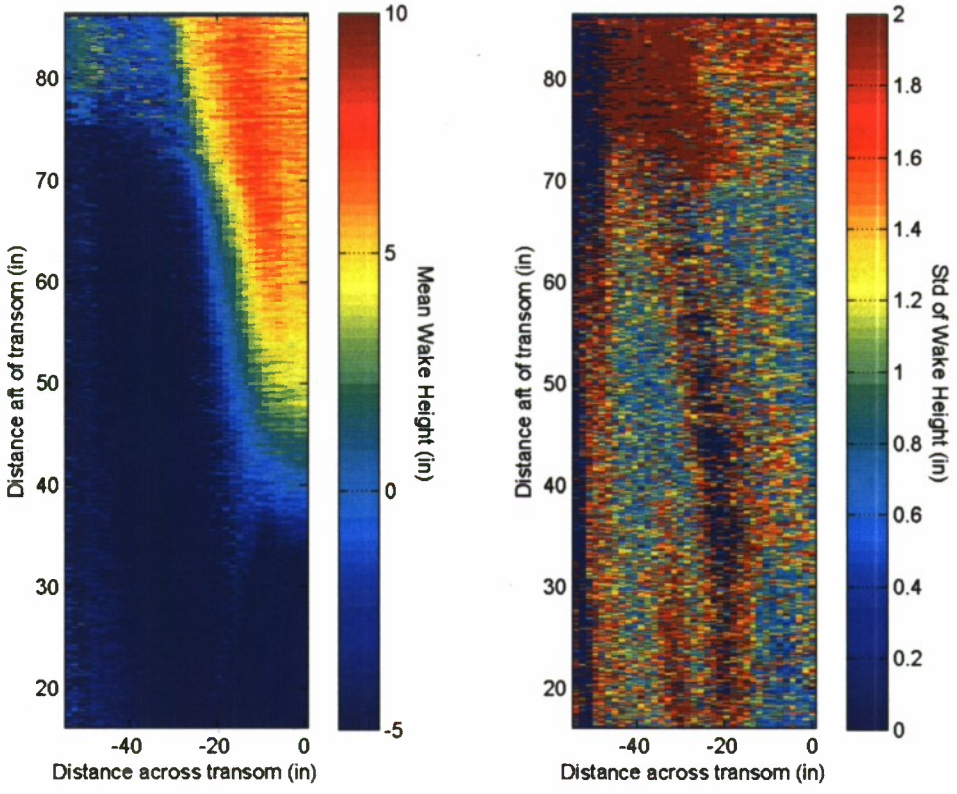

Figure 26. Surface plots of the mean and standard deviation of the wake height at a speed of 8 knots. The figure on the left is the mean wake height after it has been binned along a scan into bins of width 1.5 inches. The figure on the right is the standard deviation of the height. The statistics were computed over three repeats of each speed.

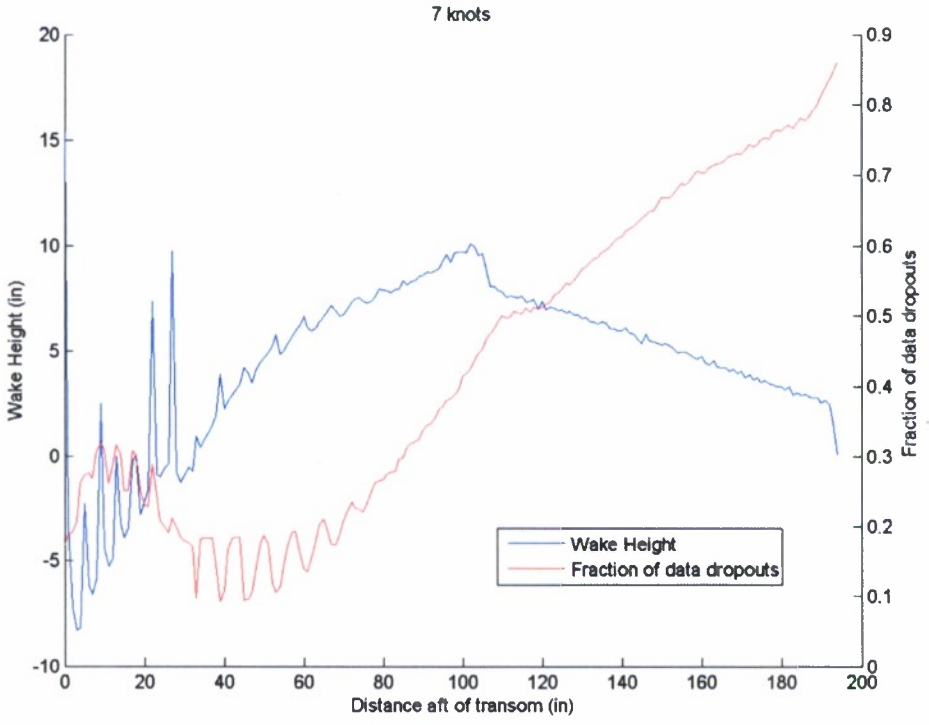

Figure 27. The mean wake height along a line 9.64 in (0.24 m) port of centerline from the LiDAR in configuration C. The red line denotes total fraction of dropouts in the LiDAR data for each measured distance aft of the transom.

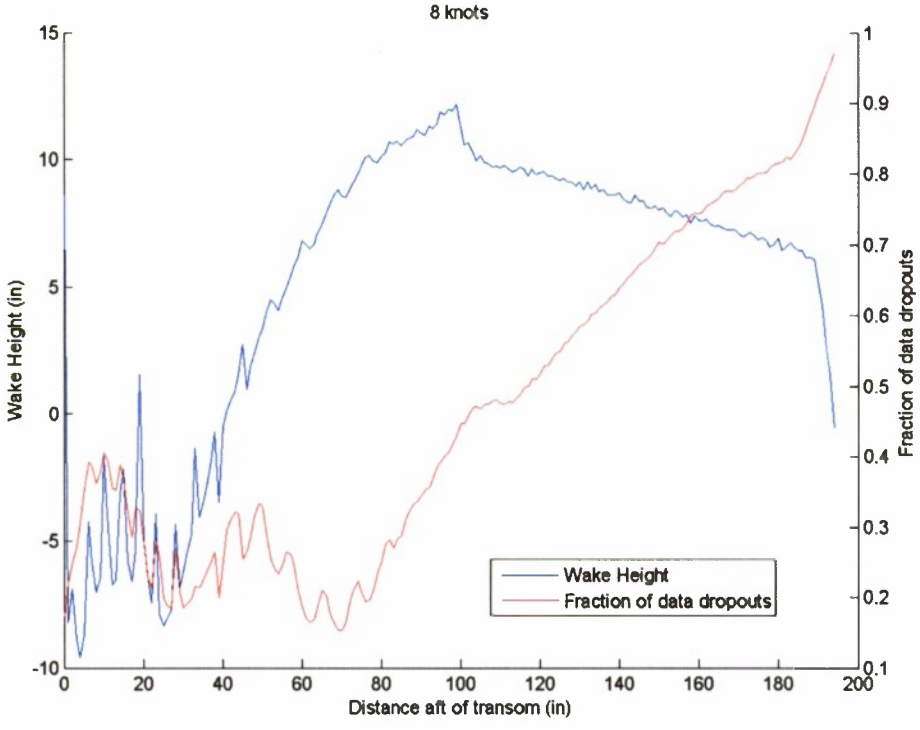

Figure 28. The mean wake height along a line 9.64 in (0.24 m) port of centerline from the LiDAR in configuration C. The red line denotes total fraction of dropouts in the LiDAR data for each measured distance aft of the transom.

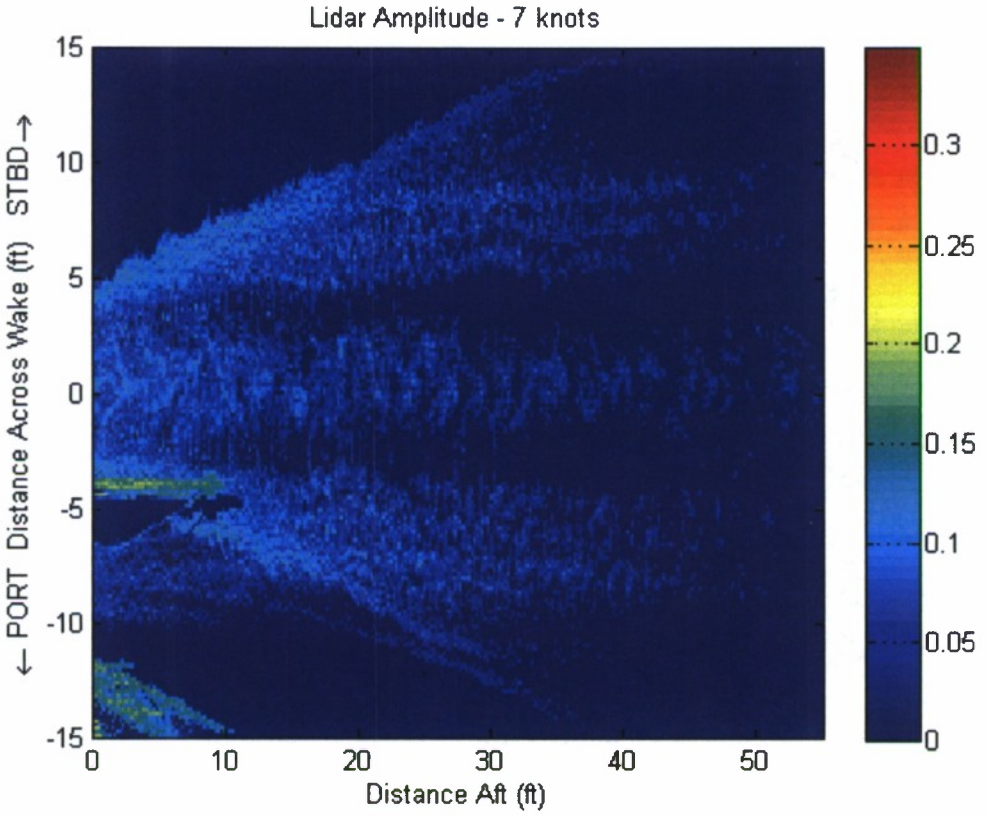

Figure 29. Image representing the strength of the return signal seen by the LiDAR at 7 knots. The warmer the color, the stronger the signal return is. The signal is mainly scattering off of foam, entrained air, and surface roughness generated by the wake.

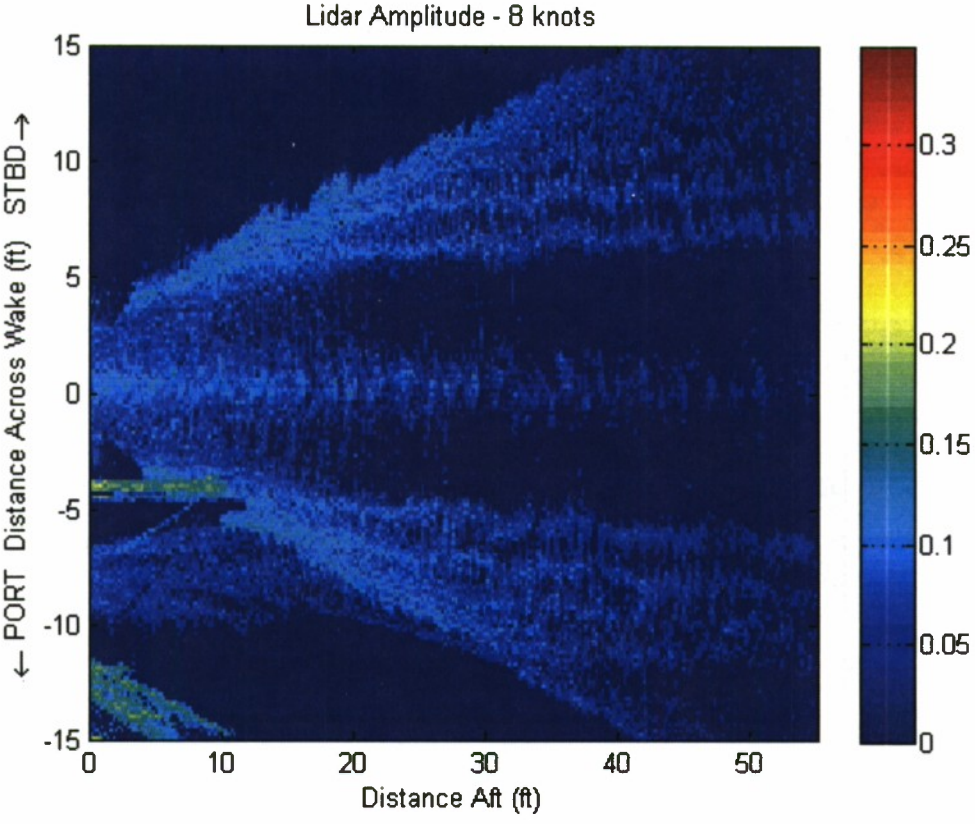

Figure 30. Image representing the strength of the return signal seen by the LiDAR at 8 knots. The warmer the color, the stronger the signal return is. The signal is mainly scattering off of foam, entrained air, and surface roughness generated by the wake.

QViz

Mean free-surface elevations were generated from raw QViz images through image processing algorithms. A method-of-moments technique was employed to identify the free surface in each image. The first and second moments can be expressed using Equations 3 and 4, respectively:

$$\bar{u}_j = \frac{\sum_{i=-h}^{h} u_i \langle I_i \rangle}{\sum_{i=-h}^{h} \langle I_i \rangle} \tag{3}$$

$$\bar{u}_j^2 = \frac{\sum_{i=-h}^{h} \left(u_i - \bar{u}_j\right) \langle I_i \rangle}{\sum_{i=-h}^{h} \langle I_i \rangle} \tag{4}$$

where u_j = location along the column of the image

u_i = location along the row of the image

I_i = the intensity of the pixel at (u_i, u_j)

h = one-half the size of the column of the image

These equations are used to determine the pixels representing the roughened free surface as well as to provide a measure of confidence in the determined value. An example is shown in Figure 31 with the complete edge detected in a raw image (left) and the edge location predicted from the first moment in a chosen image column (right).

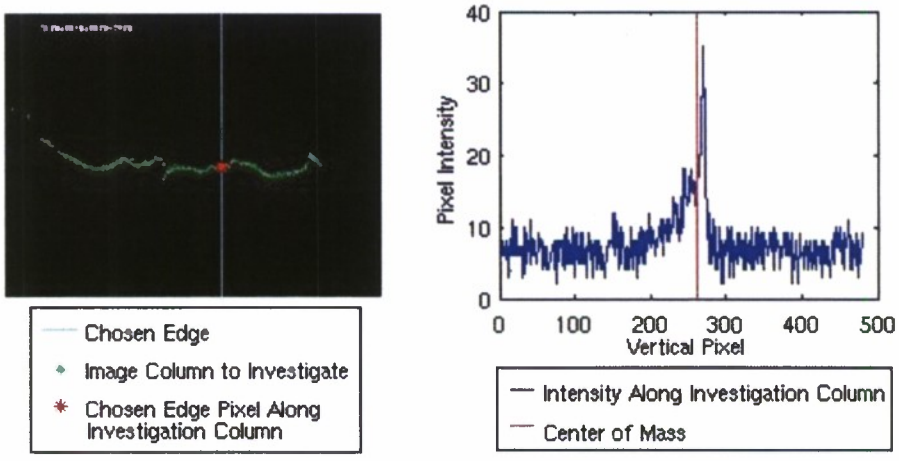

Figure 31. Example edge detection for an image collected at 7 knots, 10 in (0.254 m) aft of the transom

Figure 32 presents mean wake profiles for four transverse cuts through the wake, along with their standard deviation. The measurement variability increases aft of the transom as the wake becomes more energetic and unsteady. A minimum in the standard deviation begins to appear at the outboard edge of the measurement region where the transition location from the wake shoulder to the trough area is approached.

The spectral content of the wake was computed from the time series collected at multiple locations and is shown in Figure 33. Peaks in the spectra are evident near 1.75 Hz, which may be a characteristic of the inherent unsteadiness of the wake. Wyatt et al (8) demonstrated a similar phenomenon at 1 Hz for full-scale measurements of the R/V Athena wake.

The mean elevation field of the wake at 7 knots as measured by the QViz system is shown in Figure 34. Analysis of the 8 knot data is ongoing.

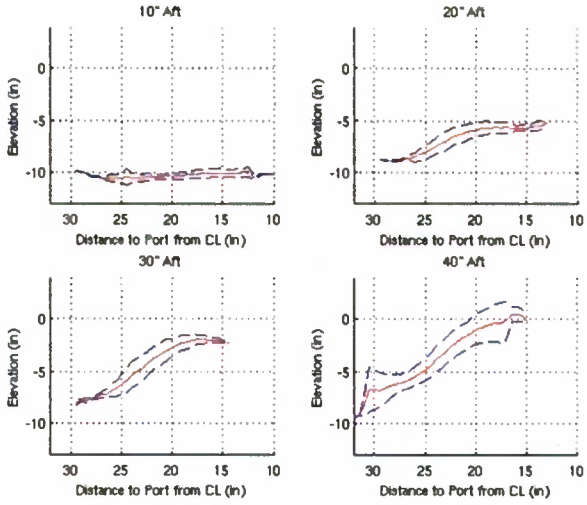

Figure 32. Transverse Cuts for QViz at four locations aft of stern for 7 knot condition.

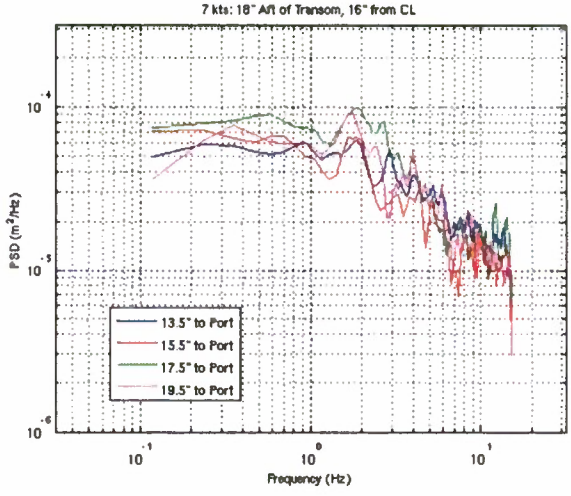

Figure 33. Power spectra of QViz measurement at 18 in (0.4572 m) aft of stern.

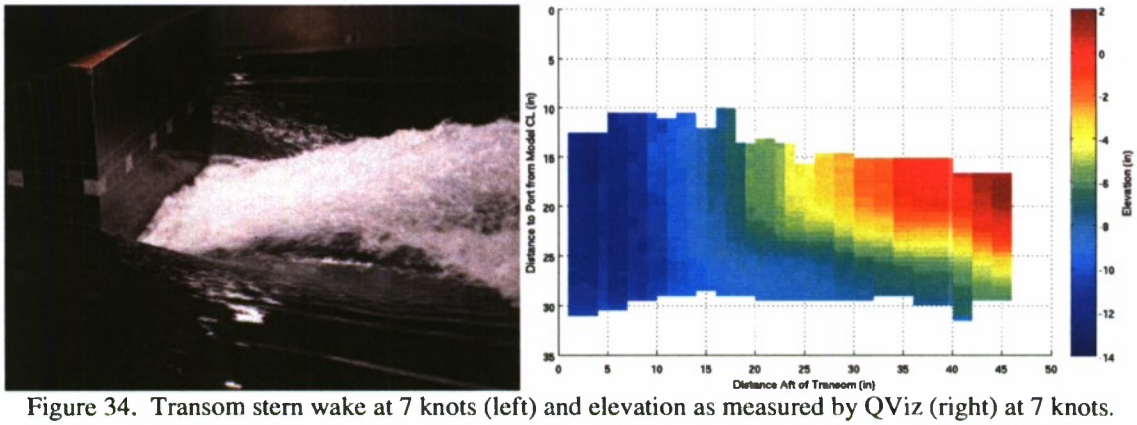

Figure 34. Transom stern wake at 7 knots (left) and elevation as measured by QViz (right) at 7 knots.

Wavecuts (Senix Ultrasonic Sensors)

The wavecut data collected using the Senix ultrasonic sensors was filtered to remove dropouts. Repeated runs were then averaged together to create a mean run for each speed at each test location. Figure 35 and Figure 36 show wavecut results for 7 knots and 8 knots, respectively, at y/B=2.37. Each plot shows the independent runs as well as the resultant averaged run.

The wave-making resistance coefficient with truncation correction was estimated using WAVECT, a Fortran routine employing the methods of (Eggers, 9) for the analysis of longitudinal wave cut measurements. Table 9 below provides the estimated wave-making coefficients along with truncation corrected coefficients at y/B = 2.37 for both the 7 and 8 knot runs.

Additional non-dimensional resistance coefficients are listed in Table 10, including the total resistance coefficients (C_t), the frictional resistance coefficients (C_f), and the residuary resistance coefficients (C_r). The total resistance coefficient was calculated using water density, model speed, measured drag force and wetted surface area. The frictional resistance coefficient is calculated using the ITTC 57 formula (PNA, 10). Residuary resistance is calculated by subtracting the frictional resistance coefficient from the total resistance coefficient. The wavemaking resistance coefficient makes up part of the residuary resistance, along with the eddy resistance. All resistance coefficients are non-dimensionalized by the static wetted surface area at the 1 foot draft, zero trim condition (132.36 ft^2, 12.3 m^2).

Figure 37 shows the non-dimensional resistance coefficients from the 2007 and 2008 tests. The total resistance coefficients were slightly higher in 2008 than 2007, which makes sense since the drag measurements also were slightly higher. Trim angles were slightly smaller and draft measurements were slightly higher at the forward perpendicular in 2008, which would cause a larger actual wetted surface area and may have contributed to the larger drag force. Measurement uncertainty may have also played a part in the difference. The wavemaking resistance coefficients were larger in 2008, which could be explained by a greater wetted surface area (displacing a larger volume of water) or measurement uncertainty. The frictional resistance coefficients were calculated the same way so the values are the same for both test years. The residuary resistance coefficients are greater in 2008 than 2007 as a result of the total resistance coefficient being of greater value.

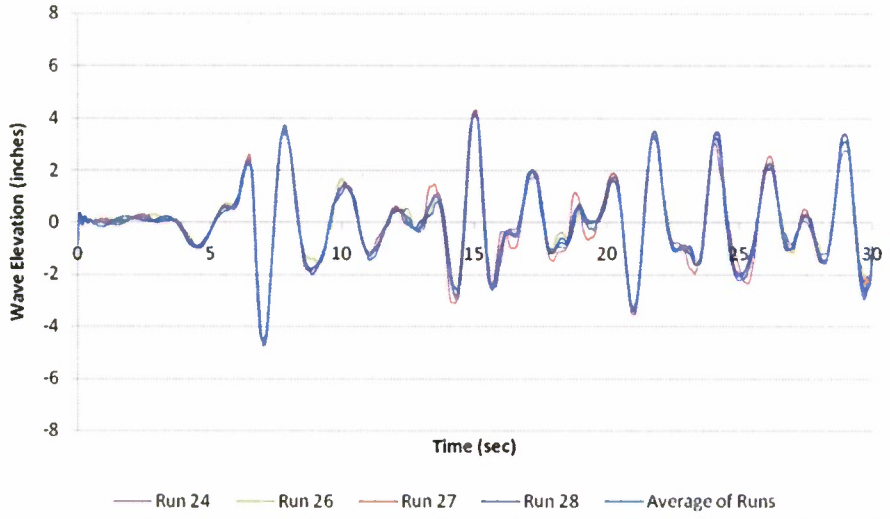

Figure 35. Four independent runs and the resultant averaged wave elevation data set at 7 knots for sonic 4 (y/B=2.37) in configuration 1.

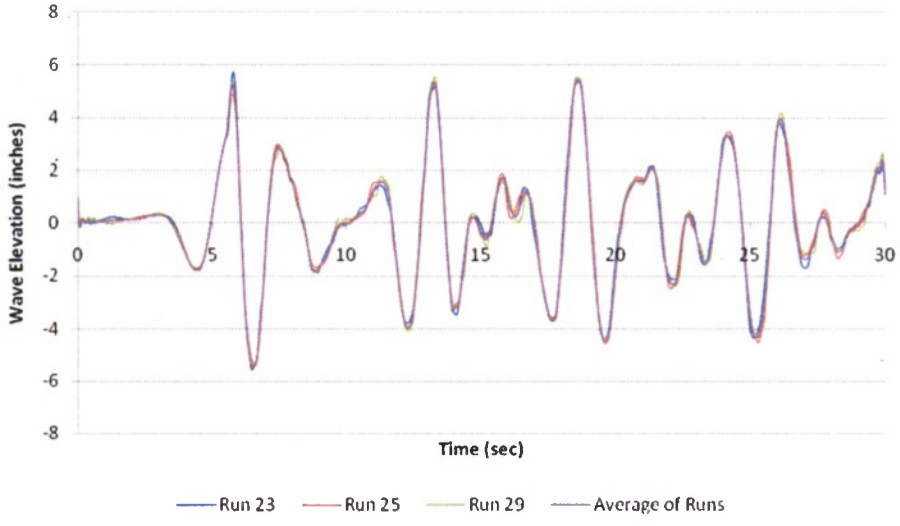

Figure 36. Three independent runs and the resultant averaged wave elevation data set at 8 knots for sonic 4 (y/B=2.37) in configuration 1.

Table 9. Calculated wave-making resistance coefficients for 7 and 8 knot runs.

Parameter	Units	7-knots	8-knots
Truncation Start	data points	957	845
	seconds	9.57	8.45
	ship lengths	3.77	3.80
Truncation End	data points	1187	1108
	seconds	11.87	11.08
	ship lengths	5.34	4.99
C_W		0.002658	0.003808
C_W, with truncation correction		0.003167	0.004036

Table 10. Non-dimensional resistance coefficients for 2008 test.

Speed	Fn_D	C_t	C_f	C_r	C_w
(kts)					
7	1.91	0.013	0.002	0.010	0.003
8	2.12	0.012	0.002	0.010	0.003

Table 11. Non-dimensional resistance coefficients for 2007 test.

Speed	Fn_D	C_t	C_f	C_r	C_w
(kts)					
5	1.43	0.0105	0.0026	0.0079	0.00001
7	1.90	0.0121	0.0025	0.0097	0.00203
8	2.10	0.0114	0.0024	0.0090	0.00278
9	2.34	0.0100	0.0024	0.0076	0.00340

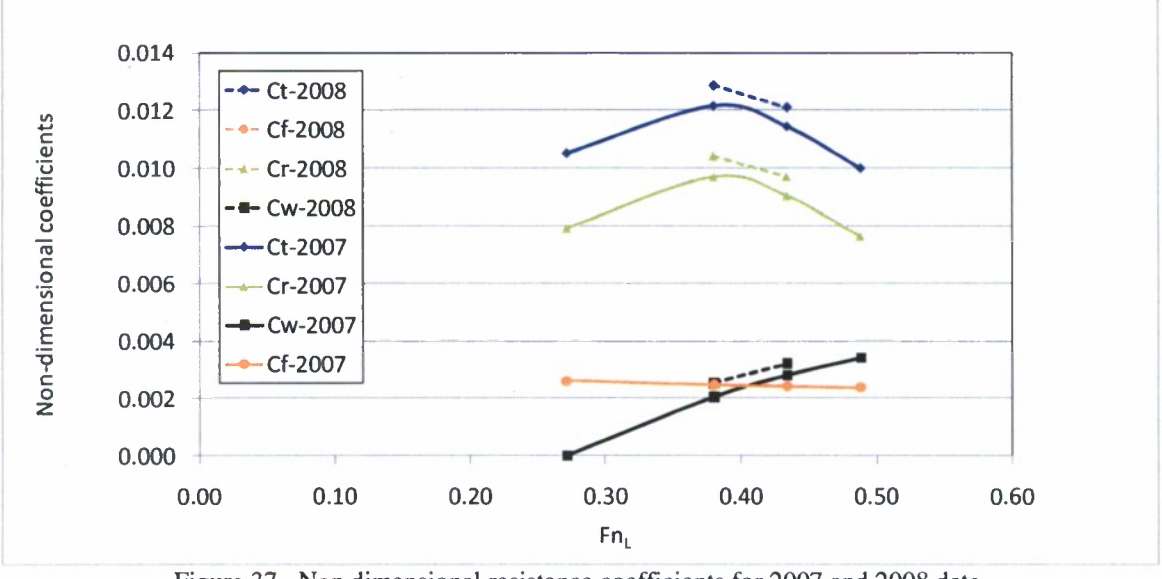

Figure 37. Non dimensional resistance coefficients for 2007 and 2008 data.

Centerline Ultrasonic Sensor

The static ultrasonic sensor collecting data along the wake at the model centerline was processed to yield maximum, minimum, and mean wave elevations along with standard deviations. Multiple measurements at the same position were averaged to obtain a single value. The moving Ultrasonic data for one run was binned into 1 in (2.54 cm) increments and data within each bin was averaged. Figure 38 shows the static and moving results for the 7 knot runs. Figure 39 shows the static and moving results for the 8 knot runs. Note that there are no measurements for the 8 knot data closer than 20 inches aft of the stern; this is because the water level dropped below the range for which the ultrasonic sensor was calibrated. A good qualitative agreement is seen between the fixed and moving ultrasonic measurements.

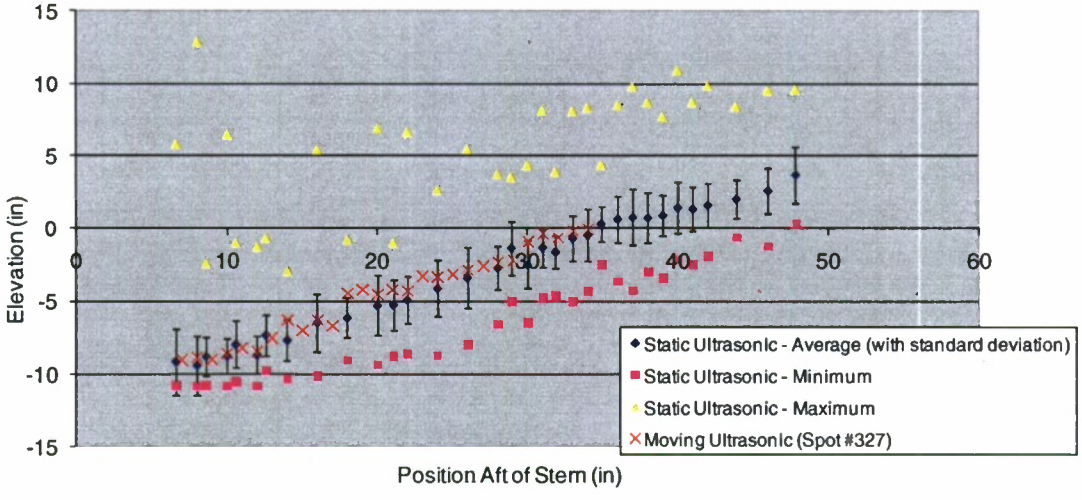

Figure 38. Centerline ultrasonic measurements at 7 knots. Positions aft are referenced to stern at 0 inches.

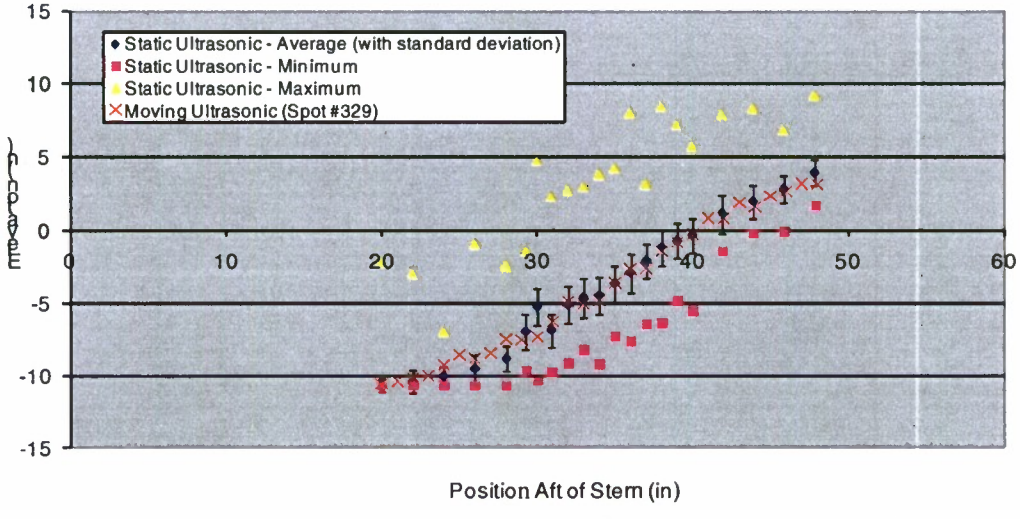

Figure 39. Centerline ultrasonic measurements at 8 knots. Positions aft are referenced to stern at 0 inches.

Acoustic Wave and Current Profiler AWAC)

Figure 40 and Figure 41 show the raw acoustic return in counts for the center beam of the AWAC while the instrument was in the centerline position. Plots are shown for both the 7 and 8 knot runs for three transverse test locations, with one figure for each speed. The black line shows the level of maximum acoustic return, which is the water surface or the bottom edge of the model. Each panel shows a single run, with time converted to distance past the stern; the forward and aft edge of the model are denoted by vertical white lines. Each panel shows one transverse location with the centerline location in the top panel, 2.5 ft (0.762 m) off centerline in the middle panel, and 5 ft (1.524 m) off centerline in the bottom panel. Though it is difficult to observe from only two speeds, AWAC results from previous testing (Fu, et. al., 1) show that more bubbles are present deeper in the water column at lower speeds than at greater speeds, assuming acoustic return is related to bubble density. These trends can be compared with the still images of the flow aft of the transom (Figure 16), which show that at 7 knots, the transom flow is relatively flat with many bubbles behind the hull. From the still photos, it appears that as the speed increases to 8 knots, the density of bubbles observed decreases, resulting in a cleaner flow with bubbles only at the surface, which tends to agree with what is seen in the acoustic return plots. The acoustic plots contain data in raw counts, so further analysis would be necessary to facilitate the direct comparison to bubble size and density.

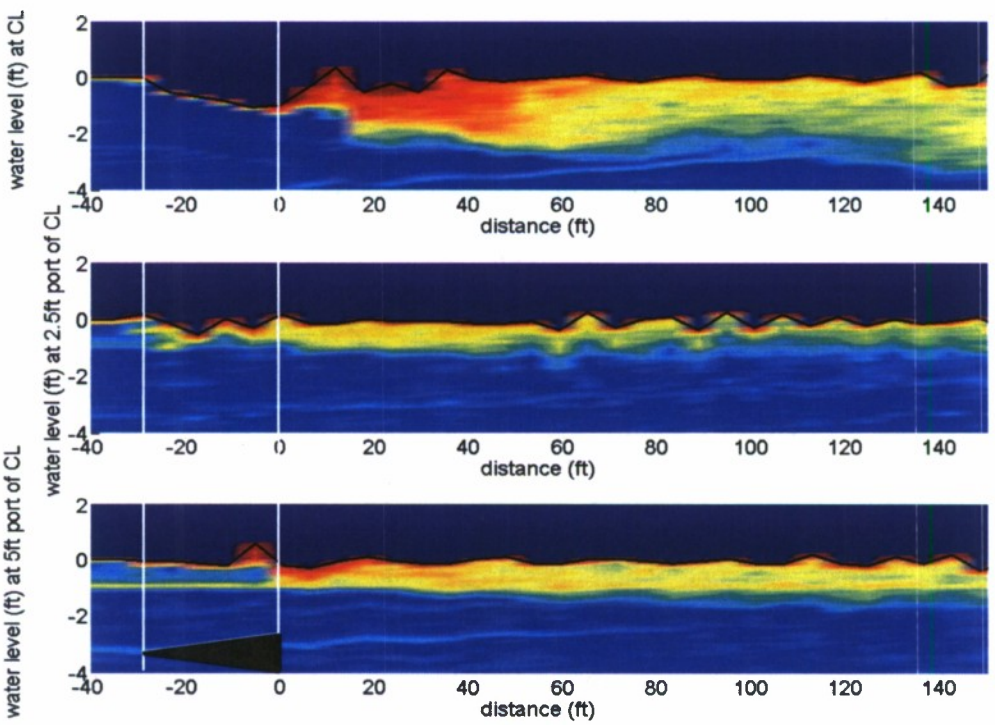

Figure 40. AWAC results for 7 knot runs. Distance is in referenee to the stern of the model at 0 ineheS.

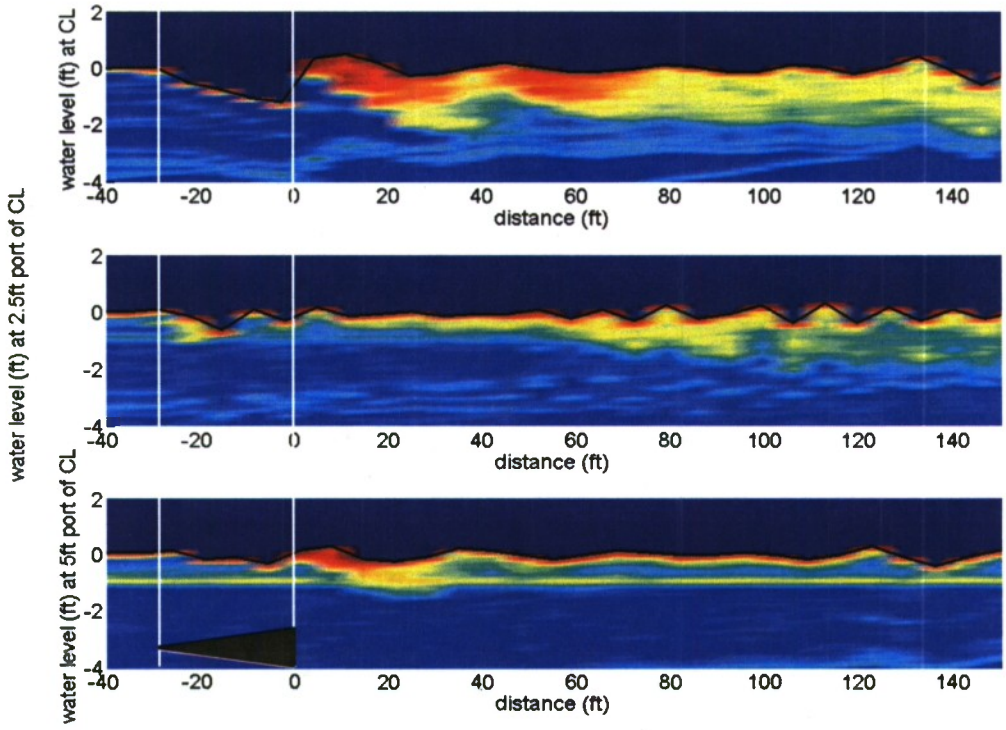

Figure 41. AWAC results for 8 knot runs. Distance is in reference to the stern of the model at 0 inches.

Defocused Digital Imagery Particle Image Velocimetry (DDPIV)

The objective of the DDPIV system was to measure air entrained by the stern wave behind the transom model. Toward this end, the camera's probe volume was placed underwater in the wake and was traversed up and down. Due to design constraints the probe volume could not be moved laterally and had limited movement longitudinally.

Images were taken at speeds of 7 and 8 knots, but these higher speeds did not show any analyzable bubbles. It is therefore presumed that the location of the camera was incorrect for measuring bubbles at these speeds. To obtain usable bubble data, runs were made at two slower speeds of 5 and 6 knots and then the data for each speed was ensemble averaged. Several thousand bubbles were measured for the ensemble and each ensemble was processed for the size distribution, bubble position distribution, and void fraction. Figure 42 shows the bubble size distribution for 5 and 6 knots with the lower speed case showing an appreciably higher average bubble size. The red bars represent the median bubble size. Figure 43 shows the void fraction distribution versus depth, indicating that the bubbles are evenly distributed in depth within our probe volume. The probe volume was closer to the free surface at higher speeds; probe depth as a function of speed is shown in Figure 44.

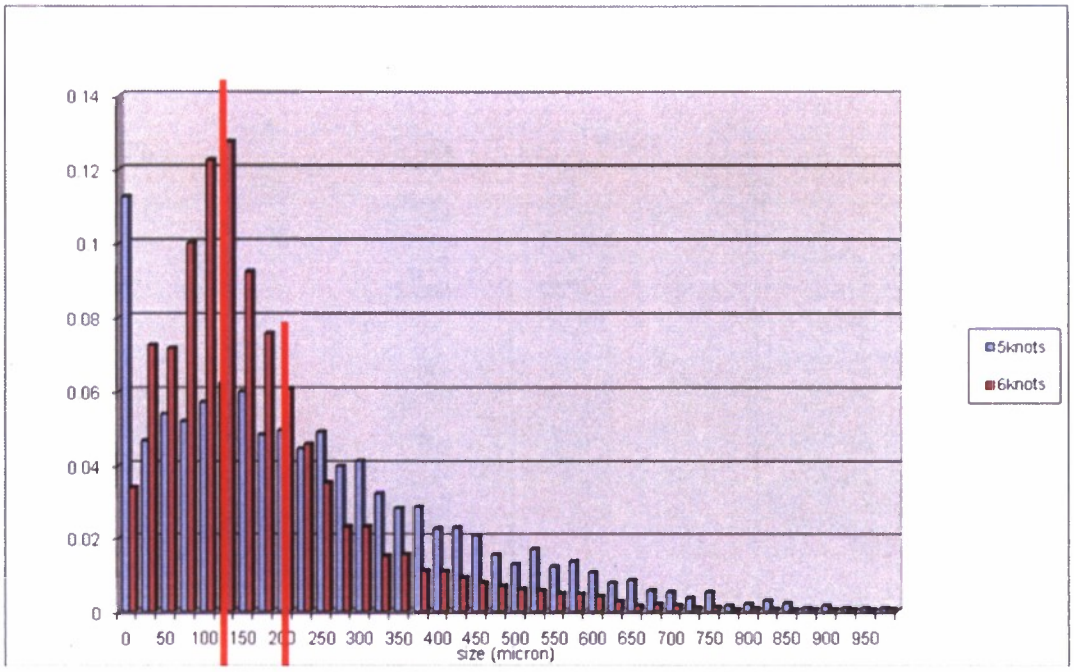

Figure 42. Bubble size distribution for DDPIV system.

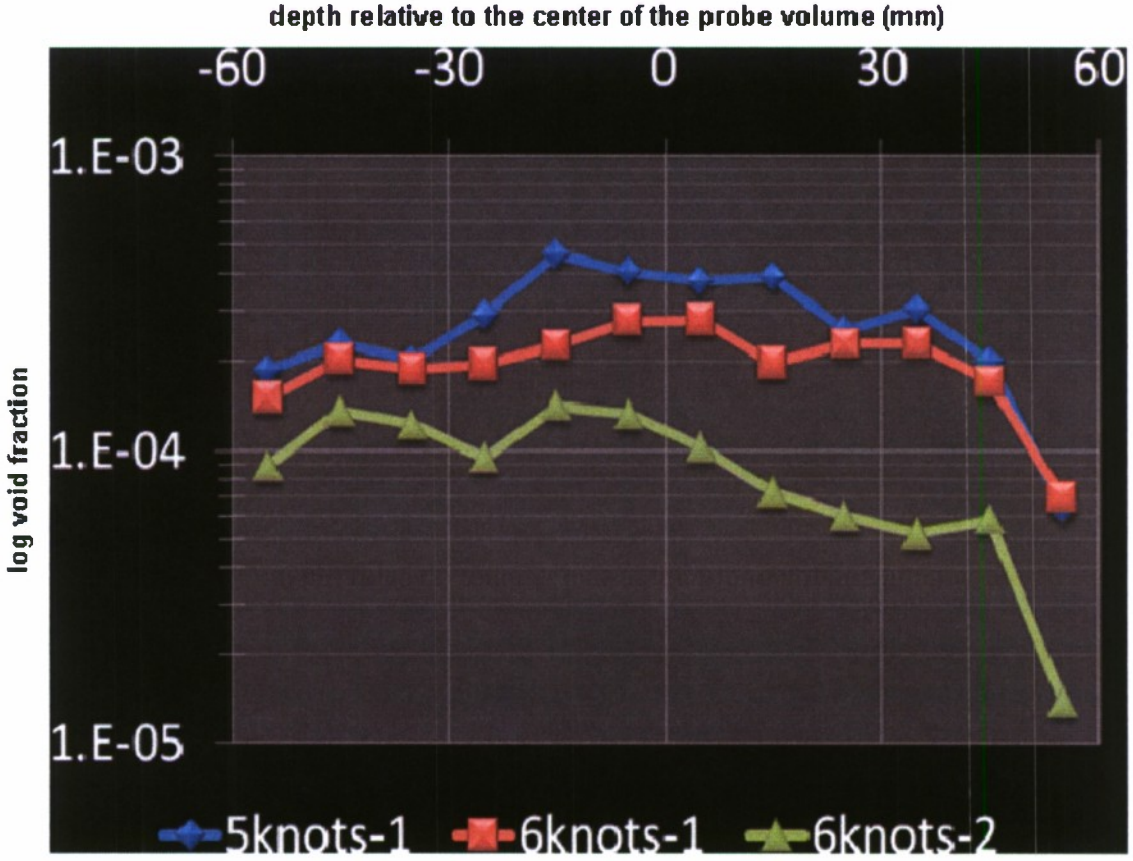

Figure 43. Void fraction as a function of depth, as measured by DDPIV system.

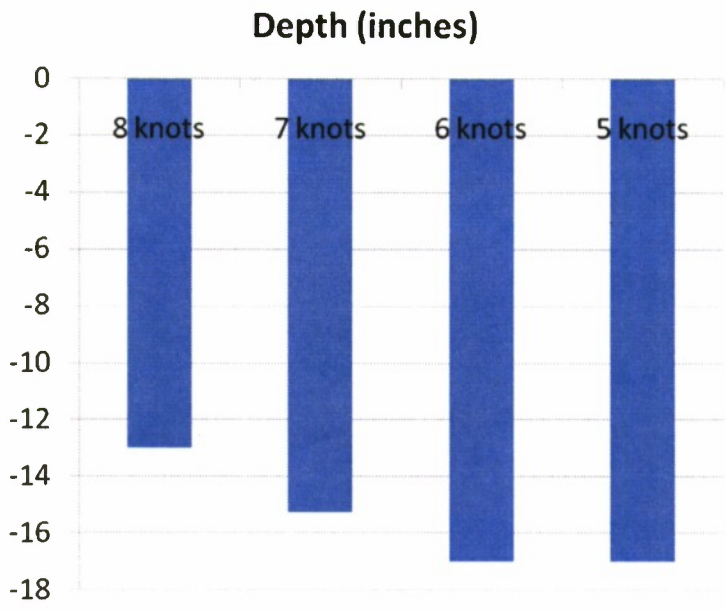

Figure 44. Depth of probe volume below free surface.

Void Fraction Probes

Figure 45 shows the wake produced at a model speed of 8 knots with the void fraction strut installed. The void fraction strut is at a longitudinal position of 41 in (1.04 m) aft of the stern and vertical position 3 (see Table 3).

Figure 45. Photograph of wake produced at 8 knots with void fraction strut attached. Void fraction probes are 41 inches (1.04 m) aft of the transom and the strut is in vertical position 3.

Due to time constraints only one repeated run of each condition was conducted. The data was processed for all runs and then the average using the duplicate runs for each condition was calculated; the averaged data is presented in this section.

Figure 46 shows a comparison of the 2007 and 2008 data. Note that the complete set of 2008 data is not shown in Figure 46; instead only data points that were repeats of the 2007 data are shown. Figure 46 shows how void fraction varies with probe height at four longitudinal distances aft of the transom. The probe heights shown along the y-axis are measured relative to calm water and the legend refers to the longitudinal distance from the probe tip to the aft of the transom in inches. The 2007 data is presented with lines connecting data points while the 2008 data is shown as only points.

The largest variation in data between the two years is at x=41 in (1.0 m) aft of the transom. This condition is the closest location to the inception of the rooster tail for which data was collected. In the 2007 data set, the measured void fraction at a probe height of -6.5 in (-0.17 m) appears to be a possible measurement error. The 2008 data collection was focused at this location for comparison and to achieve a better understanding of the flow in this area. The 2008 data provides a smoother trend than the 2007 data, which suggests that the measurement at a height of -6.5 in (0.17 m) may have been an outlier. However, the measured void fraction is consistently lower in 2008 for all probe heights above -8 in (-0.21 m), with differences of about 10% void fraction. The other significant variation between 2007 and 2008 data is at x=51 inches (1.30 m) and a probe height of 0.5 in (1.3 cm). The void fraction measured at this location and height is about 5% smaller than in 2007 and is close to the void fraction level at x=56 in (1.42 m) for the same probe height. The other data point collected at x=-1 inches (1.30 m) corresponds well with the 2007 data, so it is possible this 2008 point is a potential measurement error. Measurement errors may be due to the noise in the system as discussed previously in the description of the void fraction instrumentation.

Figure 46 also shows that up to a void fraction of approximately 12% a small change in vertical height results in a small change in void fraction. However, void fraction levels higher than 12% show that a small change in probe height results in a large change in void fraction. Assuming that a void fraction level of 50% is a rough approximate of the free surface this suggests that the void fraction level just below the free surface quickly decreases from 50% to roughly 20-25% within a vertical distance of approximately 1.75 inches (4.45 cm).

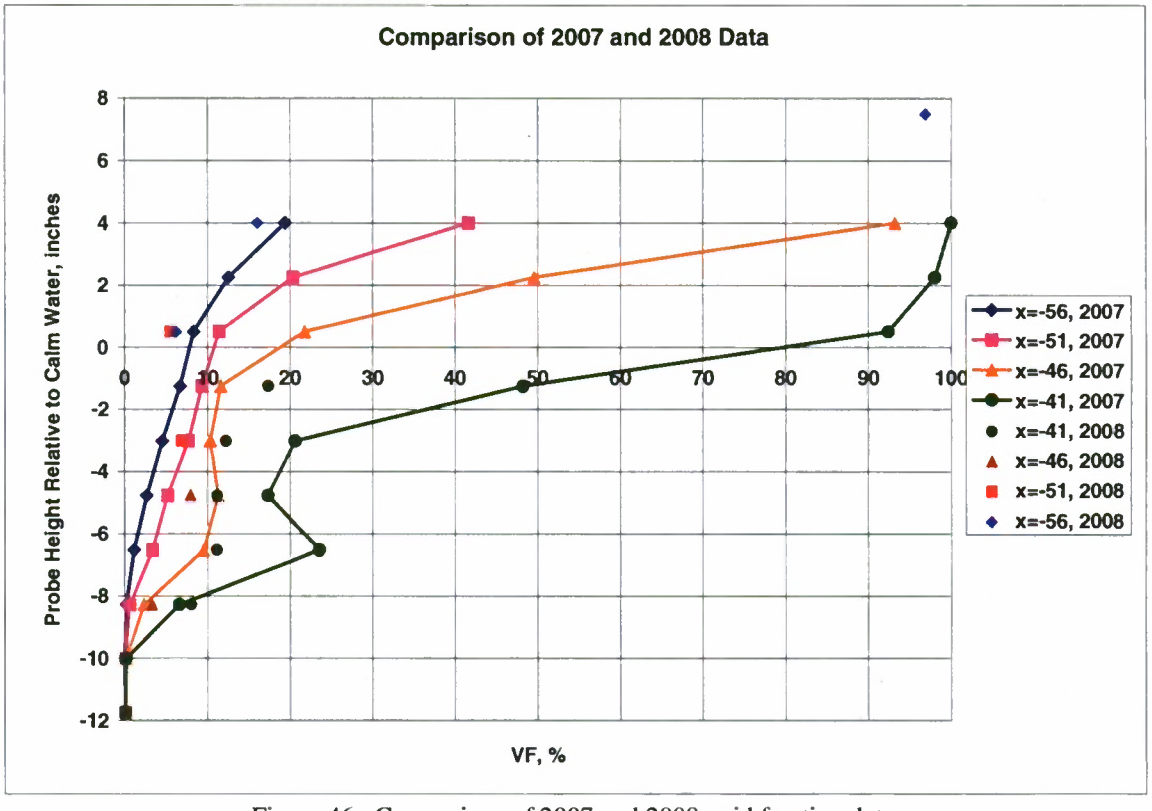

Figure 46. Comparison of 2007 and 2008 void fraction data.

Figure 47 shows a contour plot created using data merged from 2007 and 2008; a table of the merged data is provided in Table 12. Linear interpolation was used to fill gaps in the data. The contour lines represent the percent of air present in the flow with the 50% contour line as a rough approximation of the free surface. The x-axis represents the longitudinal distance relative to the transom, with negative values indicating a distance aft of the transom. The y-axis shows the probe height relative to calm water. The black dots represent the 2007 probe locations and the red dots represent 2008 probe locations.

The contour plot shows that the void fraction level at one probe height below the free surface (1.75 inches) quickly reduces from 50% void fraction at the free surface to approximately 20% void fraction. Within a span of three probe heights below the free surface the void fraction is roughly 10%. Then, with approximately every probe height below the 10% contour the void fraction decreases by roughly 2%.

There are a few peculiarities present in the contour plot. The small horizontal spike in the 7% void fraction contour at x=53.5 in (1.36 m) and probe height=0.5 in (1.27 cm) is the possible outlier mentioned in the discussion of Figure 46. Additional data spikes are obvious at x=46 in (1.17 m) and probe height -6.25 in (15.88 cm) and x=43.5 in (1.1 m), probe height -3.0 in (7.62 cm) to determine if what is shown are real characteristics of the flow. It is suspected this is a result of the crude merging of 2007 and 2008 data.

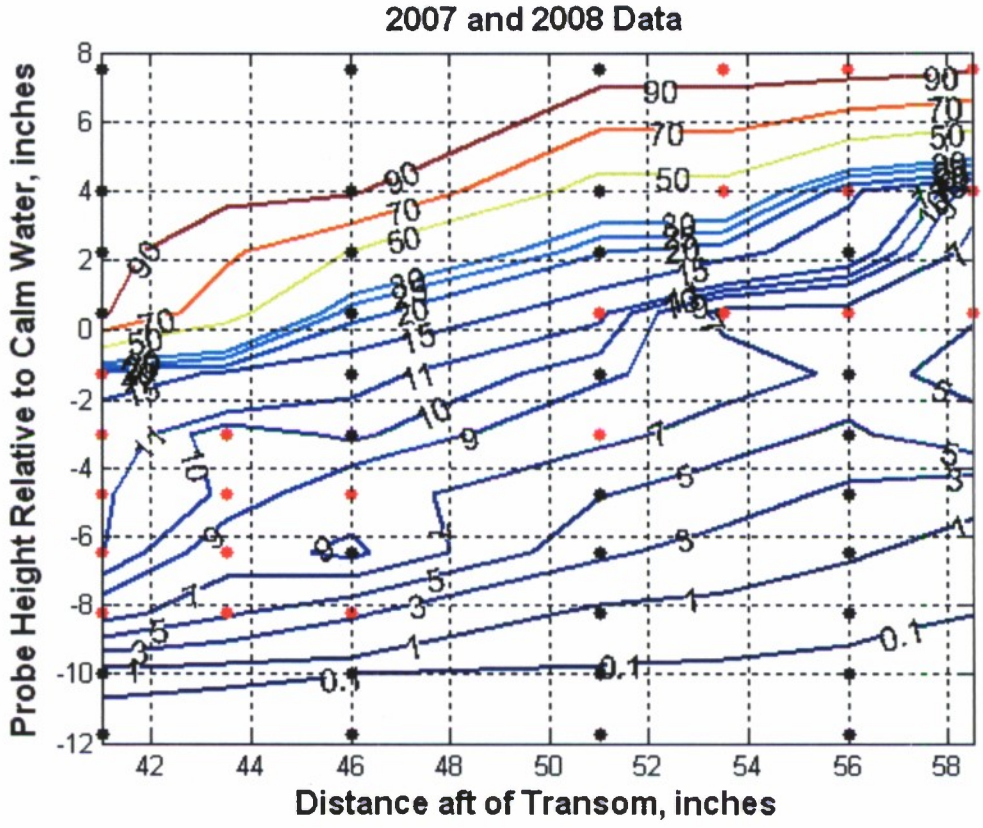

Figure 47. Void fraction contour plot using 2007 and 2008 data. Contour lines represent the percent of air present in the flow. The black dots represent 2007 data points and the red dots represent 2008 data points.

Table 12. Table of 2007 and 2008 merged data. Probe heights are measured relative to calm water.

Probe Height, inches	Longitudinal Locations, inches aft of Transom						
	41	43.5	46	51	53.5	56	58.5
7.5	99.9000	99.5000	99.0000	98.5000	98.2645	96.8420	92.6135
4	99.9470	96.5536	93.1603	41.5838	43.3810	16.0005	8.0003
2.25	97.9625	73.7478	49.5330	20.2975	16.3968	12.4960	6.2480
0.5	92.3490	57.0331	21.7173	11.3588	6.3738	6.2092	5.4548
-1.25	17.3040	14.4158	11.5275	9.3069	7.9896	6.6723	3.3362
-3	12.2025	9.1594	10.2769	7.6569	6.0829	4.5090	6.8582
-4.75	11.1445	9.8393	7.9310	5.1441	3.8941	2.6441	1.3221
-6.5	11.0895	8.0172	9.4667	3.3333	2.2315	1.1297	0.5648
-8.25	7.9937	5.3173	3.2361	0.5753	0.3883	0.2013	0.1006
-10	0.1525	0.1269	0.1013	0.0094	0.0057	0.0020	0.0010
-11.75	0.0123	0.0088	0.0052	0.0075	0.0103	0.0094	0.0047
	blue	2007 data points					
	red	2008 data points					
	black	interpolated data points					

Data Comparisons

Comparisons between the wake profiles as measured by different instrumentation are given in Figure 48 and Figure 49 for speeds of 7 and 8 knots respectively. The parallel LiDAR measurements were not collected along the centerline but are provided for completeness. All of the measurements agree well qualitatively when the parallel LiDAR results are excluded. The parallel LiDAR results for 8 knots agrees well within approximately 30 inches to 60 inches aft of the transom, while the agreement is tenuous for the 7 knot parallel LiDAR data. The observed differences are thought to be partially due to the fact that the parallel LiDAR measurements are not collected on the centerline and partially due to the large off-nadir angle of incidence . A comparison between the moving LiDAR data at the same location as the parallel LiDAR data is given in Figure 50 and Figure 51. An unexplained offset of 11 inches was found between the 2007 and 2008 data; the data presented in these plots has been corrected so that the data is in alignment.

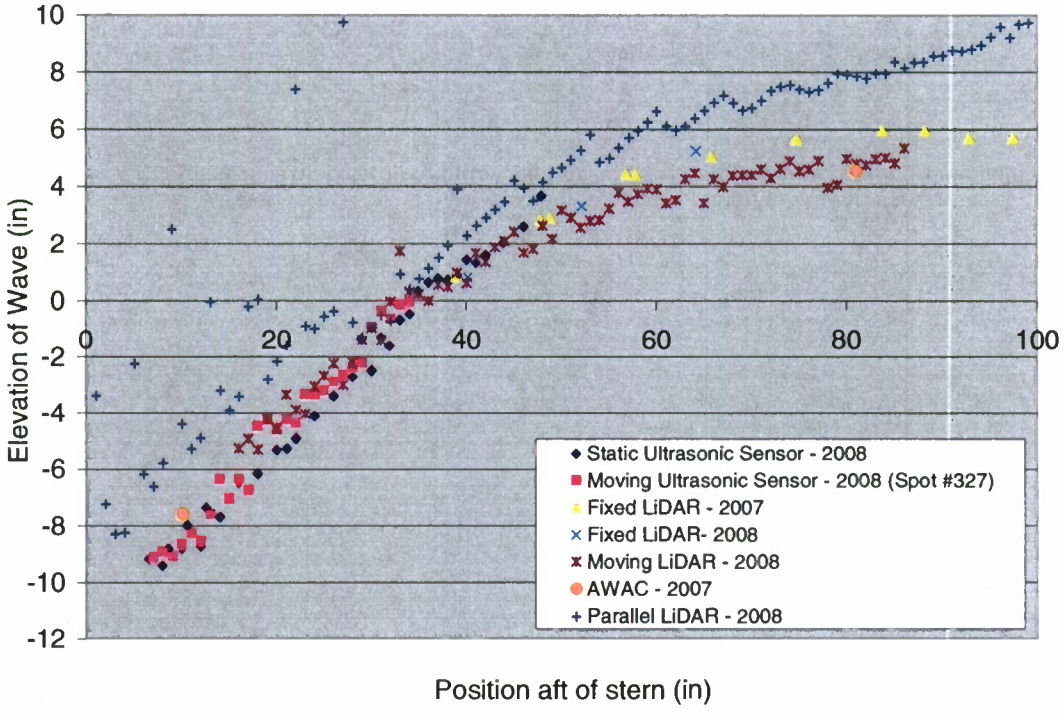

Figure 48. Centerline comparison of ultrasonic sensors, LiDAR and AWAC for 7 knot condition.

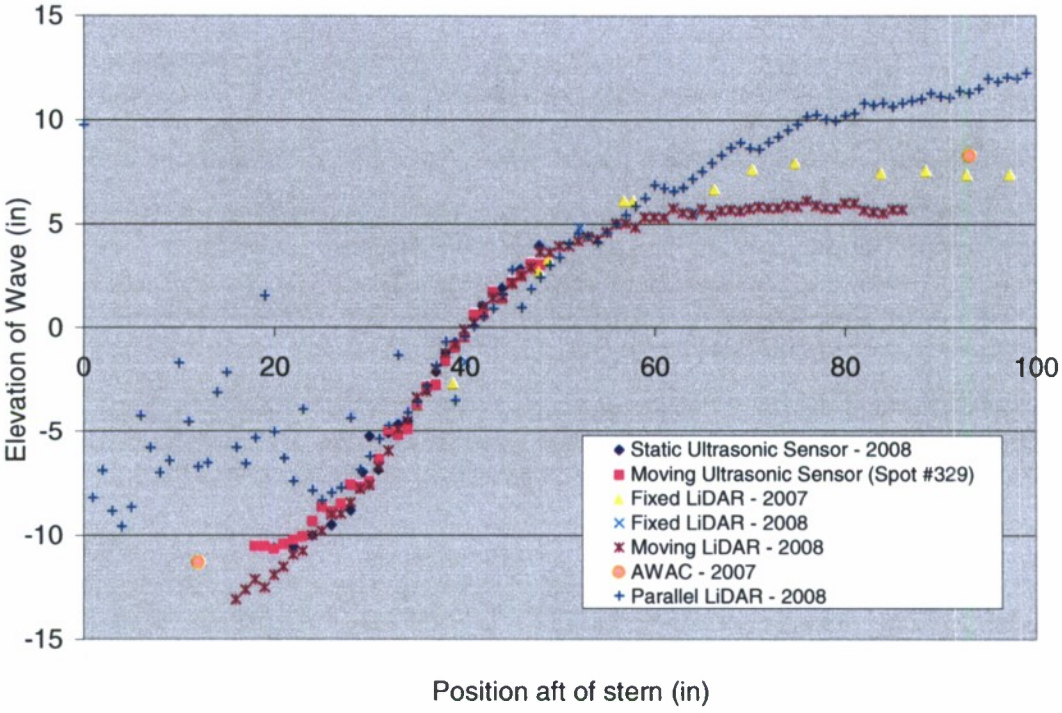

Figure 49. Centerline comparison of ultrasonic sensors, LiDAR and AWAC for 8 knot condition.

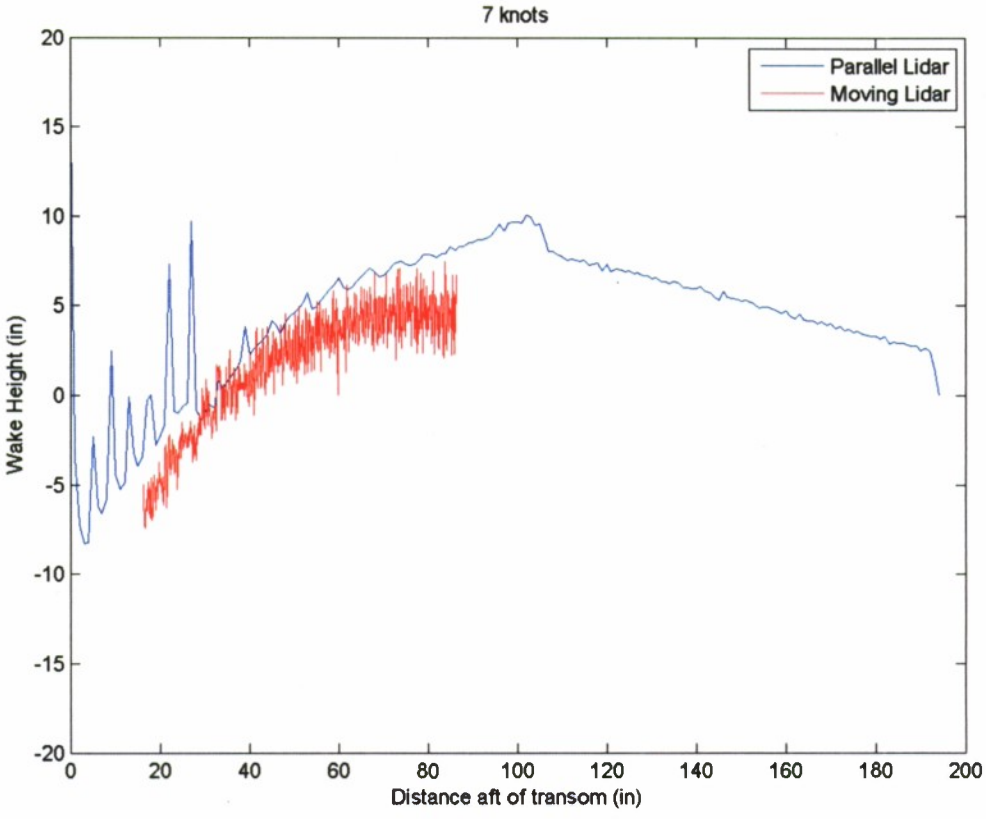

Figure 50. Comparison of the parallel LiDAR measurements at 7 knots with moving LiDAR data taken along a line 9.644 inches (0.24 m) to port of the transom centerline.

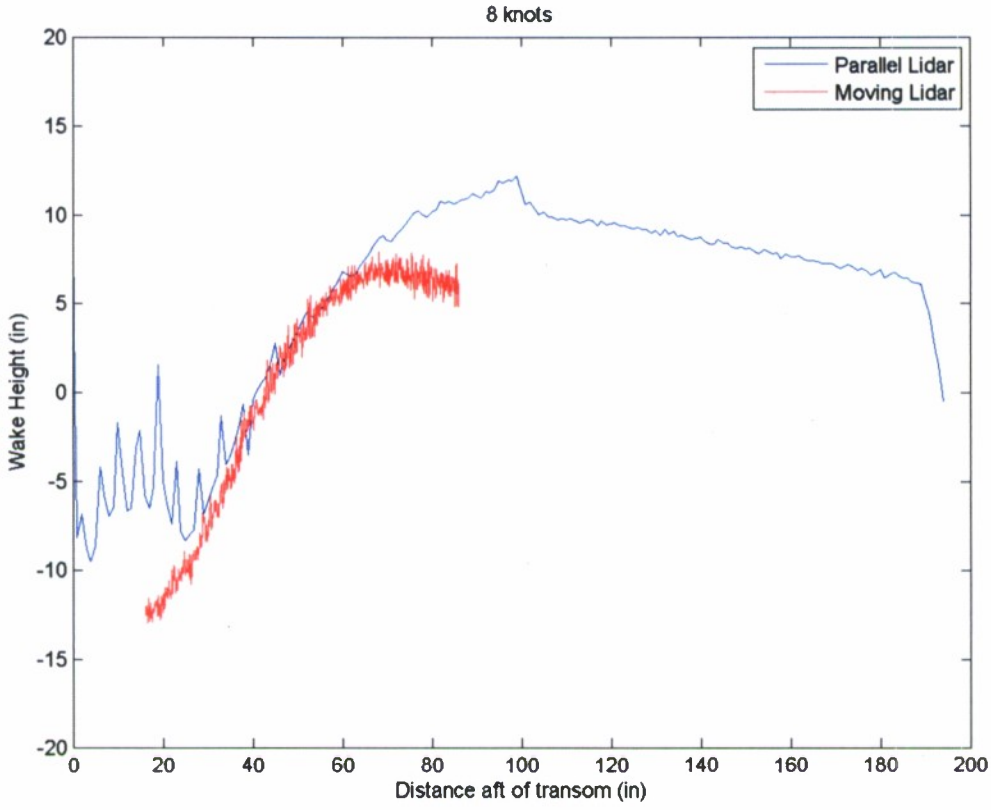

Figure 51. Comparison of the parallel LiDAR measurements at 8 knots with moving LiDAR data taken along a line 9.644 inches (0.24 m) to port of the transom centerline.

The LiDAR measurements of 2007 and 2008 are compared with QViz measurements of 2008 in Figure 52, Figure 53, Figure 54 and Figure 55. Figure 52 and Figure 53 provide a comparison between the QViz measurements and the 2007 LiDAR data. The QViz data is shown above the LiDAR data with the two measurements separated by a white line and there is good qualitative agreement between the datasets. Figure 54 and Figure 55 show a comparison between the 2007 and 2008 moving LiDAR data. The 2008 LiDAR data is displayed on the starboard side of the transom centerline and it's extent is denoted by white lines. Again there is good qualitative comparison between the two measurements. The data in the figures were adjusted for the fore/aft offset of 11 inches, but there may still be slight fore/aft discrepancies in the two datasets due to errors from determining the longitudinal extent of each moving LiDAR run. Additionally the 2007 data was collected at a number of discrete locations aft of the transom and averaged over a run, and was then interpolated to have an interline spacing of 2 in (0.05 m). It is not unexpected therefore for the 2007 data to appear "smoother" when compared with the 2008 data collected from a continuously moving LiDAR during the course of a run.

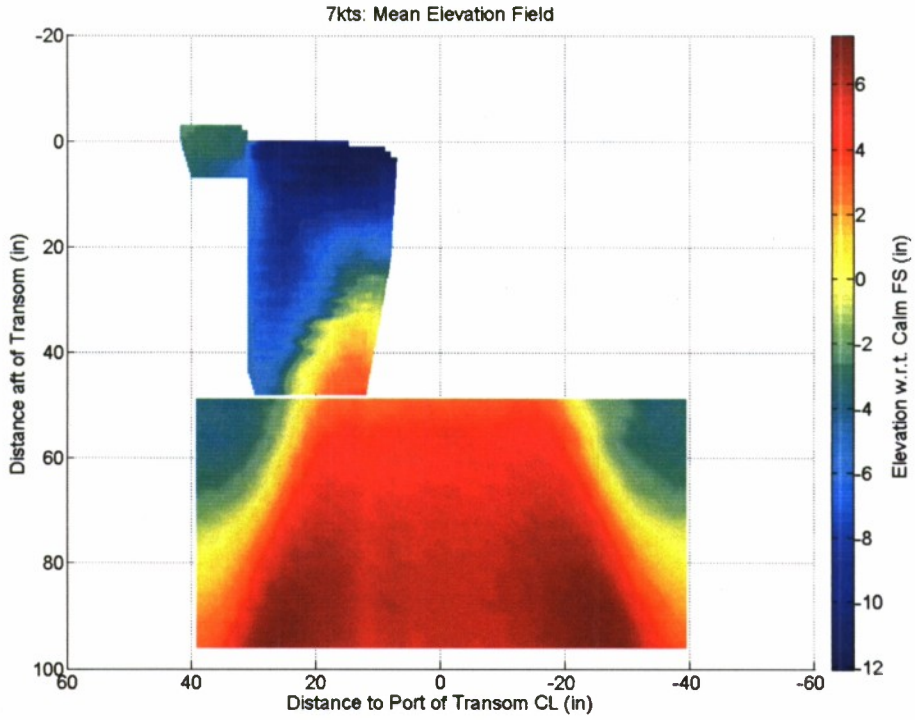

Figure 52. Surface contour comparison of QViz (2008) and LiDAR (2007) data for 7 knots. The boundary between QViz and LiDAR data is denoted by a white line.

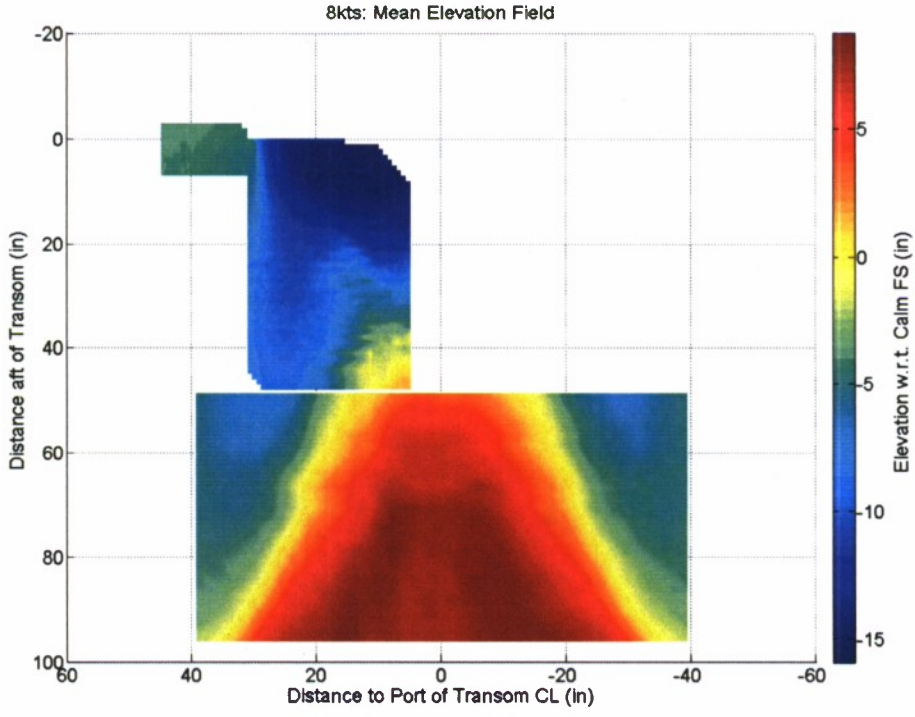

Figure 53. Surface contour comparison of QViz (2008) and LiDAR (2007) data for 8 knots. The boundary between QViz and LiDAR data is denoted by a white line.

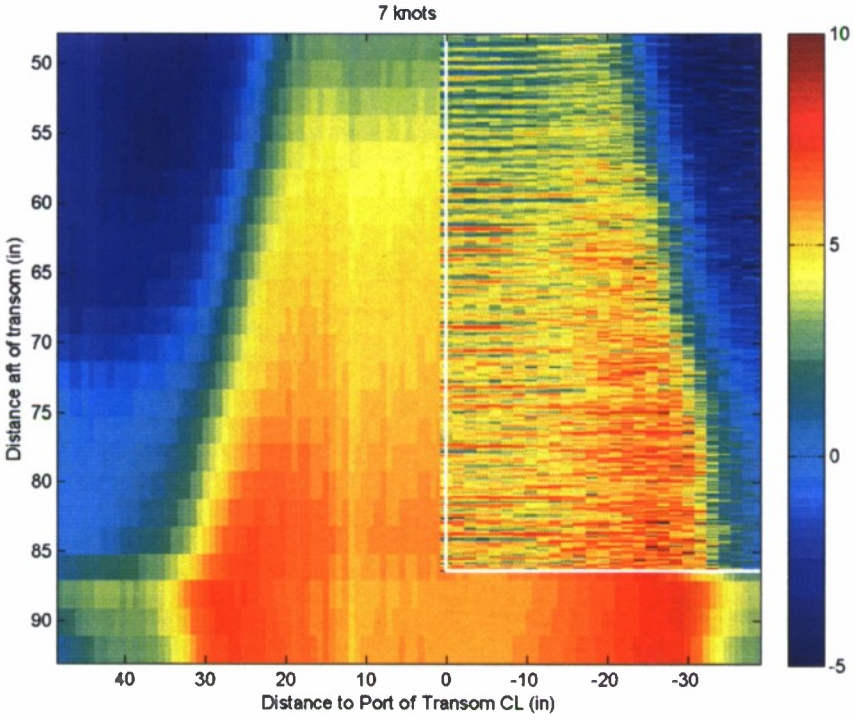

Figure 54. Comparison of LiDAR measurements from 2007 and 2008 (inset) for a speed of 7 knots. Boundary of the 2008 data is denoted by a white line.

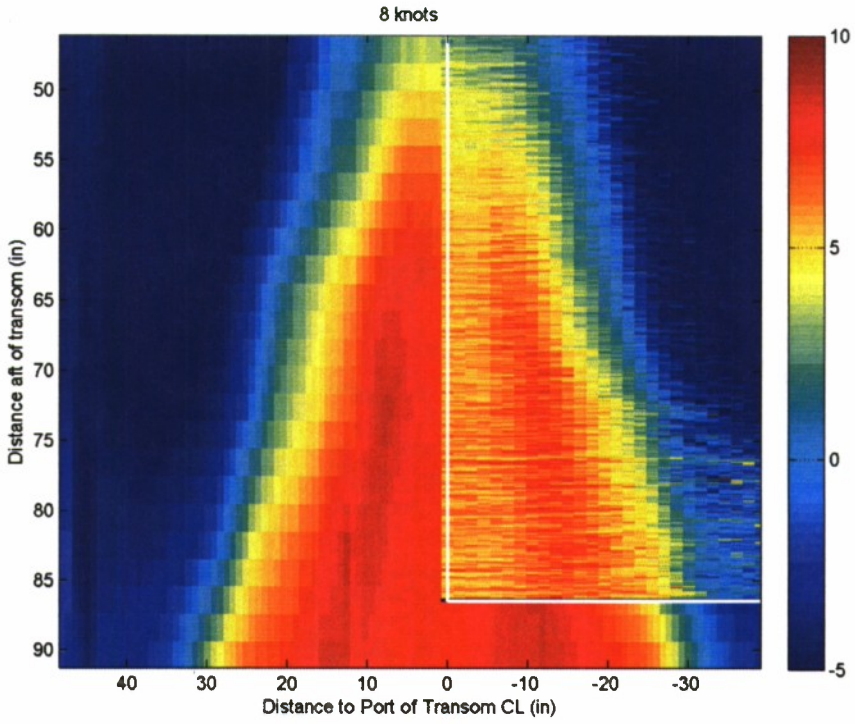

Figure 55. Comparison of LiDAR measurements from 2007 and 2008 (inset) for a speed of 8 knots. Boundary of the 2008 data is denoted by a white line.

CONCLUSIONS

A laboratory model capable of producing full-scale transom breaking waves similar in behavior to those of full-scale naval combatants has been designed, fabricated and tested. Multiple measurement methods have been implemented and presented, and comparisons between the still images of the wake and the LiDAR data, AWAC data and void fraction data agree well qualitatively. The initial experimental work to document and characterize a large breaking transom wave in calm water over a range of transom depth Froude numbers has been completed, and analysis of data continues to provide further comparisons between measurements, as well as insight into the physics of the transom stern wave.

REFERENCES

1. Fu, T., Fullerton, A.M., Ratcliffe, T., Minnick, L., Walker, D., Pence, M.L. and Kirk Anderson. "A Detailed Study of Transom Breaking Waves," Hydromechanics Department Report, NSWCCD-50-TR–2009/025, May 2009.

2. Saunders, H. E. "The David W. Taylor Model Basin, Parts 1, 2 & 3," SNAME Transactions Volumes 46, 48 & 49, 1938, 40 & 41.

3. Maki, K. J., Doctors, L. J. and R. F. Beck. "On the Profile of the Flow Behind a Transom Stern." *Ninth International Conference on Numerical Ship Hydrodynamics,* Ann Arbor, MI, 2007.

4. Faltinsen, O. *Hydrodynamics of High-Speed Marine Vehicles.* Cambridge University Press, New York, 2005.

5. Furey, D.A., and Fu, T.C. "Quantitative Visualization (QViz) Hydrodynamic Measurement Technique of Multiphase Unsteady Surfaces," *Proceedings of the 24th Symposium on Naval Hydrodynamics*, Office of Naval Research, 2002.

6. Rice, J.R., Walker, D.C., Fu, T.C., Karion, A. and T. Ratcliffe. "Quantitative Characterization of the Free-Surface Around Surface Ships," *Proceedings of the 25th Symposium on Naval Hydrodynamics*, Office of Naval Research, 2004.

7. Waniewski, T.A. "Air Entrainment by Bow Waves," Ph.D Thesis, California Institute of Technology, Pasadena, CA, 1999.

8. Wyatt, D.C., T.C. Fu, G.L. Taylor, E.J. Terrill, T. Xing, S. Bhushan, T.T. O'Shea, and D.G. Dommermuth, "Comparison of Full-Scale Experimental Measurements and Computational Predictions of the Transom-Stern Wave of the R/V/ Athena I," 27th Symposium on Naval Hydrodynamics, Seoul, KOREA, 5 - 10 October 2008

9. Eggers, K.W.H., Sharma, S.D., and Ward, L.T.W. "An assessment of some experimental methods for determining the wavemaking characteristics of a ship" SNAME Transactions, Vol. 75, 1967, 112-144

10. *Principles of Naval Architecture: Volume II-Resistance, Propulsion and Vibration.* Society of Naval Architects and Marine Engineers, Jersey City, New Jersey, 1988.

This page intentionally left blank.

DISTRIBUTION LIST

Copies		Name
3	SAIC	Chevalier, Dommermuth, Wyatt (pdf only)
2	CalTech	Gharib, Jeon (pdf only)
2	Iowa	Stern, Carrica (pdf only)
NAVSEA		
1	DTIC	
ONR		
1	331	Purtell
Division Distribution		
1	3452	Library (pdf only)
1	5060	Walden
5	5600	Anderson, Drazen, Minnick, Ratcliffe, Russell (pdf only)
2	5700	Brewton, Gorski (pdf only)
5	5800	Fu, Fullerton, Walker (pdf only), Files (2)